



Bastian Friesenbichler BSc.

**Investigation of different cations in
organic/inorganic tin halide perovskites for solar cell
applications**

Master Thesis

To achieve the university degree

Diplom Ingenieur

Masterstudium Advanced Material Sciences

Submitted to

Graz University of Technology

Supervisor

Assoc. Prof. DI Dr. Gregor Trimmel

Institute for Chemistry and Technology of Materials

Graz University of Technology

AFFIDAVIT

I declare that I have authored this thesis independently, that I have not used other than the declared sources/resources, and that I have explicitly indicated all material which has been quoted either literally or by content from the sources used.

The text document uploaded to TUGRAZonline is identical to the present master's thesis.

EIDESSTATTLICHE ERKLÄRUNG

Ich erkläre an Eides statt, dass ich die vorliegende Arbeit selbstständig verfasst, andere als die angegebenen Quellen/Hilfsmittel nicht benutzt, und die den benutzten Quellen wörtlich und inhaltlich entnommenen Stellen als solche kenntlich gemacht habe. Das in TUGRAZonline hochgeladene Textdokument ist mit der vorliegenden Masterarbeit identisch.

Graz, _____

ABSTRACT

Tin-based perovskites have drawn a lot of attention in the last years to the perovskite solar cell community and have made big advances in the last 5 years from starting below 3 % in 2012 up to 6.2 % in late 2016 to now 9 % in late 2017. This work focuses on the investigation of new Sn-based perovskite for use in solar cell applications. Different amounts and combinations of A-side cations in $ASnI_3$ perovskites have been investigated to get information on promising new materials. Solar devices were manufactured in an inverted setup, extended with an anti-solvent dropping step, and were tested with various perovskite absorber layers of the structure $ASnI_3$. (A = Cs, MA, FA, $PEA_{0.2}Cs_{0.8}$, $PEA_{0.2}MA_{0.8}$, $PEA_{0.2}FA_{0.8}$, $MA_{0.75}FA_{0.25}$, $MA_{0.75}FA_{0.15}PEA_{0.1}$)

The influence of the different A-cations has been studied in terms of solar cell performance, optical and crystallographic properties, and long term stability. In terms of optical and crystallographic properties, the experimental data of the fabricated $MASnI_3$, $FASnI_3$ and $MA_{0.75}FA_{0.25}SnI_3$ perovskites is in accordance with already published literature, proving the possibility of obtaining those materials with the used method. However, the resulting solar cell performance was far from reported values for the same materials. Moreover, in all cases the influence of PEA^+ as performance enhancing cation was investigated and proved.

Furthermore, the most notable finding originating from these experiments was the fabrication and characterization of the triple cation tin perovskite $MA_{0.75}FA_{0.15}PEA_{0.1}SnI_3$. This newly formed perovskite material exceeded its double cation equivalent in terms of efficiency and long-term stability by far, obtaining an efficiency value of 5.6% over almost two weeks. With this data, the enhancing effect of PEA^+ can be seen clearly in all solar cell characteristics.

Finally, another result of this thesis was the influence of the quality of the used chemicals, especially the essential SnI_2 . This study compared the solar cell performance of devices utilising SnI_2 , purchased and self-synthesised, as well as chemicals purified via a resublimation route, for perovskite absorber layers.

KURZFASSUNG

Perovskit-Solarzellen auf der Basis von Zinn haben in den letzten 5 Jahren großes Interesse geweckt, da sich ihre Effizienz rapide gesteigert hat, von 3 % in 2012 über 6.2 % Ende 2016 bis zu aktuellen 9 % in 2017. Das Ziel dieser Arbeit ist die Erforschung neuer Sn-basierender Perovskite zur Anwendung in der Photovoltaik. Verschiedenste Kombinationen, hinsichtlich Art und Anteil, von A-Kationen in Perovskiten der Struktur $ASnI_3$ wurden untersucht, um Informationen über neue vielversprechende Materialien zu erhalten. Die Solarzellen wurden in einem inversen Aufbau, kombiniert mit einem Anti-solvent Schritt, mit verschiedenen absorbierenden Perovskitschichten der Form $ASnI_3$ (A = Cs, MA, FA, $PEA_{0.2}Cs_{0.8}$, $PEA_{0.2}MA_{0.8}$, $PEA_{0.2}FA_{0.8}$, $MA_{0.75}FA_{0.25}$, $MA_{0.75}FA_{0.15}PEA_{0.1}$) hergestellt und getestet.

Der Einfluss von A-Kationen wurde in Bezug auf Solarzellenleistung, Langzeitstabilität sowie optische und kristallographische Eigenschaften hin untersucht. Hinsichtlich optischer und kristallographischer Eigenschaften waren die experimentellen Daten der hergestellten MA_3SnI_3 , FA_3SnI_3 und $MA_{0.75}FA_{0.25}SnI_3$ Perovskiten in Übereinstimmung mit bereits veröffentlichter Fachliteratur, was die Möglichkeit der Herstellung dieser Materialien mit dieser Methode bewies. Jedoch lagen diese in Bezug auf ihre Solarzellenleistung weit unter den veröffentlichten Werten. Des Weiteren wurde in allen Fällen, der positive Einfluss von PEA^+ auf die Effizienz in Solarzellen untersucht und bewiesen.

Darüber hinaus wurde, als wohl wichtigste Erkenntnis dieser Experimente, der Perovskit $MA_{0.75}FA_{0.15}PEA_{0.1}SnI_3$ hergestellt und charakterisiert. Dieses neue Perovskitmaterial übertraf alle anderen Perovskite, die in dieser Arbeit untersucht wurden, in Bezug auf Solarzellenleistung und Langzeitstabilität bei weitem und behielt seine Effizienz von 5.6% über einen Zeitraum von beinahe zwei Wochen. Anhand dieser Daten konnte der leistungssteigernde Effekt von PEA^+ in allen Solarzellencharakteristika erkannt werden. Ein weiterer Teil der Arbeit war der Einfluss der Qualität der verwendeten Ausgangschemikalie SnI_2 . In dieser Arbeit wurden Solarzellen hinsichtlich ihrer Effektivität verglichen, welche kommerzielles, selbst synthetisiertes und selbst, mittels einer Resublimationsroute aufgereinigtes SnI_2 als Ausgangschemikalie für die Perovskitschichten verwendeten.

ACKNOWLEDGEMENT

I want to thank Assoc. Prof. Dr. techn. Dipl. Ing. Gregor Trimmel for giving me the opportunity to write my master thesis at the Institute of chemical Technology of Materials and for the supervision of my work.

I further want to thank Dr. techn. Dipl. Ing. Thomas Rath, Dipl. Ing. Sebastian Höfler BSc, Dipl. Ing. Stefan Weber BSc and Benjamin Kain BSc for their ideas, input and help during the time of my research.

Also, I want to thank the whole working group of Prof. Trimmel, for the good atmosphere and the kind environment.

Further, I want to thank Mrs. Birgit Kunert for doing the XRD measurements.

In addition, I want to thank the Project PERMASOL in cooperation with Austrian Institute of Technology, Johanneum Research and the University of Patras.

Also, I want to thank Mrs. Sophie Mills, for her assistance on my experiments, during her ERASMUS internship.

Furthermore, I want to thank my parents for their support during my whole academic education, without whom this would not have been possible.

Finally, I want to thank Mrs. Tamara Wiedenegger for the moral support during my master thesis.

ABBREVIATIONS

AZO	aluminium doped zinc oxide
CIGS	Cu(InGa)Se ₂
DMF	<i>N,N</i> – dimethyl formamide
DMSO	dimethyl sulfoxide
DSSC	dye sensitized solar cell
E_g	Band gap energy
EQE	external quantum efficiency
ETL	electron transport layer
FA	formamidinium
FF	fill factor
FTO	fluorine doped tin oxide
HOMO	highest occupied molecular orbital
HTL	hole transport layer
I_{mmp}	current at maximum power point
I_{sc}	short circuit current
ITO	indium doped tin oxide
IV	current-voltage
J_{sc}	short circuit current density
LUMO	lowest unoccupied molecular orbital
MA	methyl ammonium
MMP	maximum power point
P3HT	poly-(3-hexylthiophen-2,5-diyl)
PC₆₀BM	[6,6]-phenyl-C ₆₁ -butyric acid methyl ester
PCE	power conversion efficiency
PEA	phenethyl ammonium
PEDOT:PSS	poly(3,4-ethylenedioxythiophene):polystyrene sulfonate
PMMA	poly(methyl methacrylate)
PSC	Perovskite solar cells
PV	Photovoltaic
Spiro-MeOTAD	<i>N,N,N',N',N'',N''',N''''</i> -Octakis(4-methoxyphenyl)-9,9'-spirobi[fluorene]-2,2',7,7'-tetramine
TCO	transparent conductive oxide
TFSC	thin film solar cells
V_{mmp}	voltage at maximum power point
V_{oc}	open circuit voltage

TABLE OF CONTENTS

Abstract	III
Kurzfassung	IV
Acknowledgement.....	V
Abbreviations	VI
1 Introduction.....	1
1.1 Worldwide energy demand and renewable resources	1
1.2 Solar energy as renewable energy	1
2 Theoretical Background	3
2.1 Basic Introduction into solar cells	3
2.1.1 Working principle of solar cells	3
2.1.2 Characterisation of solar cells	6
2.2 Types of solar cells.....	9
2.2.1 Silicon solar cells.....	9
2.2.2 Thin film solar cells	10
2.2.3 Multi-junction cells	12
2.2.4 Organic solar cells.....	13
2.2.5 Dye sensitized solar cell.....	15
2.2.6 Perovskite solar cells	17
2.3 General Overview of perovskite solar cells	18
2.3.1 Lead based perovskite solar cells	18
2.3.2 Lead – free perovskite solar cells	19
2.4 Tin-based perovskite solar cells.....	22
2.4.1 State of the Arts research on Sn-perovskites	22
2.4.2 Introduction of PEA ⁺ and its role in 2D perovskite formation	24
2.4.3 Aim of this thesis	25
3 Experimental	26
3.1 Chemicals.....	26
3.2 Purification of purchased SnI ₂	26
3.3 Synthesis of SnI ₂	26
3.4 Precursor Solutions	27
3.5 Device fabrication.....	28
3.6 Measurements and characterisation	29
4 Results and Discussion	31

4.1	Single Cation Sn–perovskites.....	31
4.1.1	Optical characterisation	31
4.1.2	XRD analysis.....	33
4.1.3	Solar cell performance	35
4.2	Double cation Sn–perovskites.....	37
4.2.1	Optical characterisation	37
4.2.2	XRD analysis.....	39
4.2.3	Solar cell performance	39
4.3	Introduction of PEA ⁺ Cation.....	40
4.3.1	Changes in optical properties.....	41
4.3.2	XRD analysis.....	43
4.3.3	Solar cell performance	44
4.4	Triple Cation Sn – Perovskite.....	46
4.4.1	Optical characterisation	47
4.4.2	XRD analysis.....	48
4.4.3	Solar cell performance	49
4.4.4	EQE measurement.....	51
4.4.5	Hysteresis behaviour	52
4.5	First stability tests	53
4.6	Investigation of organic cation combinations	55
4.7	Influence of SnI ₂ purity on solar cell performance.....	56
5	Conclusion and Outlook	58
6	Literature.....	60
7	Index of figures.....	68
8	Index of Tables	70

1 INTRODUCTION

1.1 WORLDWIDE ENERGY DEMAND AND RENEWABLE RESOURCES

World primary energy demand has grown by an annual average of around 1.8% since 2011, with wide variations from countries and regions, especially fast growing in development countries. Growth in primary energy demand has occurred largely in developing countries, whereas in developed countries it has slowed or even declined. All renewable energy sources combined made in 2016 up to 19.3 % of this demand. One important use of this produced energy is as electricity. Renewable sources like hydropower, wind, bio power, solar photovoltaic (PV) and others made up 24.5% of the Global electricity production in 2016. ¹ (Fig. 1)

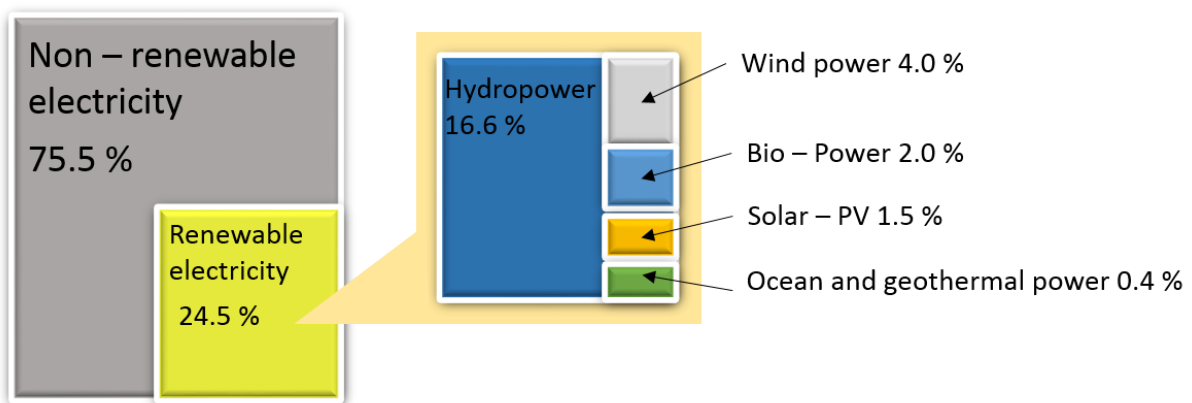


Figure 1: Renewable energy share of Global electricity production. End 2016

The world now adds more renewable power capacity annually than it adds capacity from all other fossil fuels combined. In 2016, renewables accounted for an estimated nearly 62% of additions to global power generating capacity. By the end of 2016, renewables made up for an estimated 30% of the world's power generating capacity.¹

1.2 SOLAR ENERGY AS RENEWABLE ENERGY

Solar energy can occur in various forms: as solar heat, solar photovoltaic, solar thermal electricity and solar fuels. It can be a promising alternative to fossil fuels and can contribute a lot to solving some of the most urgent problems of the world nowadays: climate change, energy security, and universal access to stable and affordable power grids. Solar energy has

many advantages: It is climate-friendly, clean, inexhaustible and a very abundant energy resource to humanity. Moreover, solar energy sources are relatively well spread over the globe. Its availability is even greater in warm and sunny countries, which will experience the most growth in population and economic development in the next decades. Solar energy has become more and more affordable and competitive in terms of cost in the last decades. Solar power, harnessed from solar thermal electricity and PV electricity, is already a major competitor to oil-fuelled electricity generation, in countries with high solar radiation and on small islands. One important advantage of solar PV is, that it can be easily installed in small and large scale, close to the customer, for example rooftops and building walls. In developing country, where a stable electric grid is not always well established, as well as in countries with well developed power grids, solar power can ensure a greater net stability and security.² Solar PV was the world's leading source of additional power generating capacity in 2016. The annual market increased by 75 Gigawatt-direct current (GWdc), which relates to 50% increase in the last year, to now a total of 303 GWdc.

The top country in adding annual renewable electricity source in 2016 was China, with 85% of additions, leading the board, followed by USA, Japan and India.¹

2 THEORETICAL BACKGROUND

2.1 BASIC INTRODUCTION INTO SOLAR CELLS

2.1.1 Working principle of solar cells

Solar cells or PV cells are, generally speaking, devices made from a semiconducting material that has the possibility to convert light into electric energy. The conversion is realised by the absorption of photon energy, emitted by a light source, like the sun or artificial light. The absorbed photon energy excites crystal atoms, thereby generating negative charged electron and positive charged “holes”.³ The term “hole” came from the figurative assumption that an electron leaves the valence band of a material and generates a “free spot”. The real case is that there is no “hole”; just the missing electron is generating a positive charge in the semiconductor valence band. In inorganic semiconductors the electrons and holes are mainly free charges, whereas in organic semiconductors the charges form an electron–hole–pair, or exciton.⁴ This exciton can be separated in its free charge carriers, which can further be transported in the material to the next neighbouring atom and so forth on to a current collector, provided charge carrier mobility is present in the material. Charge carriers transport is normally driven by Brownian motion, where the separated electrons and holes never move far from each other. When electrons and holes come close to each other, they may recombine to gain charge neutrality, emitting light or creating heat in the process. However, when charge carriers experience an electric field, electrons tend to drift towards the anode and holes tend to drift towards the cathode. Therefore, an electrical circuit can be closed and a device can be powered, since recombination occurs in the external circuit. To achieve the required built-in field, a “doped” semiconductor is needed. In doping processes, one part of the semiconductor is mixed with a small amount of “impurities” to change the electrical properties. The region of the crystal that is doped with an electron donating species is called a *n*-type semiconductor, (e.g. phosphorus in silicon) whereas the crystal region doped with electron accepting impurities (e.g. boron in silicon) is called a *p*-type semiconductor.³ By putting together those materials one creates a p–n–junction. (Fig. 2)

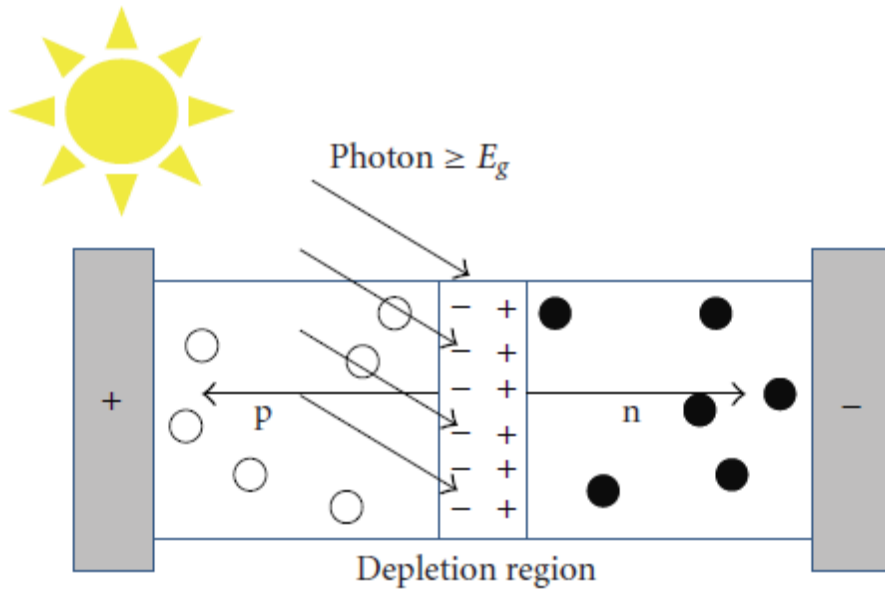


Figure 2: Basic scheme of a p–n–junction solar cell and charge transport phenomena⁵

The p–n–junction can be described in a simplified model with the conduction band of a semiconductor populated by free electrons and the valence band populated by free holes. The doping of the semiconducting material shifts the Fermi–level, closer to the conduction band in case of an *n*–type doping and closer to the valence band in case of *p*–type doping. When the system is in thermodynamic equilibrium the Fermi–levels are aligned through the crystal, inducing a bending in both bands and creating the built-in field.³ When photons with higher energy than the band gap energy values are absorbed by the semiconductor it creates an electron hole pair, which is separated, due to the built-in field.⁵ Electrons on the *p*–type side will “roll down” the energetic hill and holes in the *n*–type side will “crawl up” the energetic difference. (Fig. 3)^{3,6}

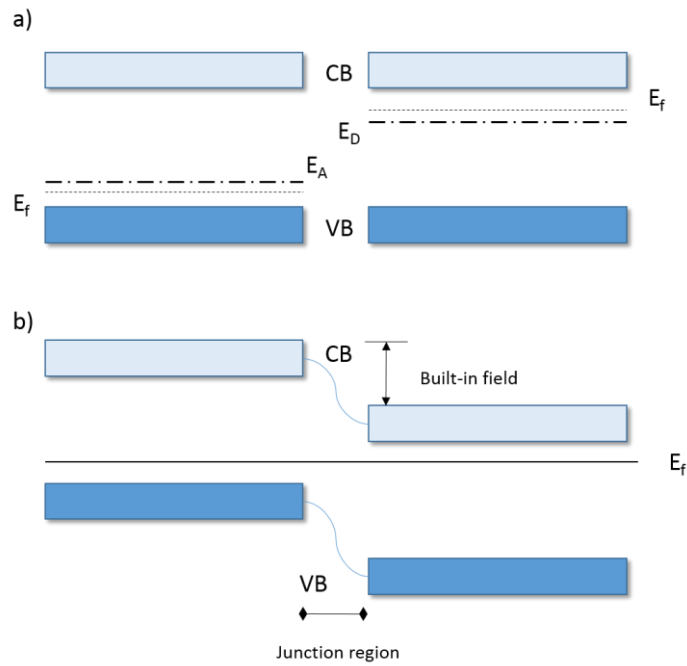


Figure 3: p–n–junction with Fermi–levels changed by doping (a) and alignment when in contact (b)

Contrarily to this in organic semiconductor solar cells, the main charge carrier transport mode is diffusion from a zone of high charge carrier concentration to a zone of low charge carrier concentration, driven by an electrochemical potential gradient. (Fig. 4)^{7,8}

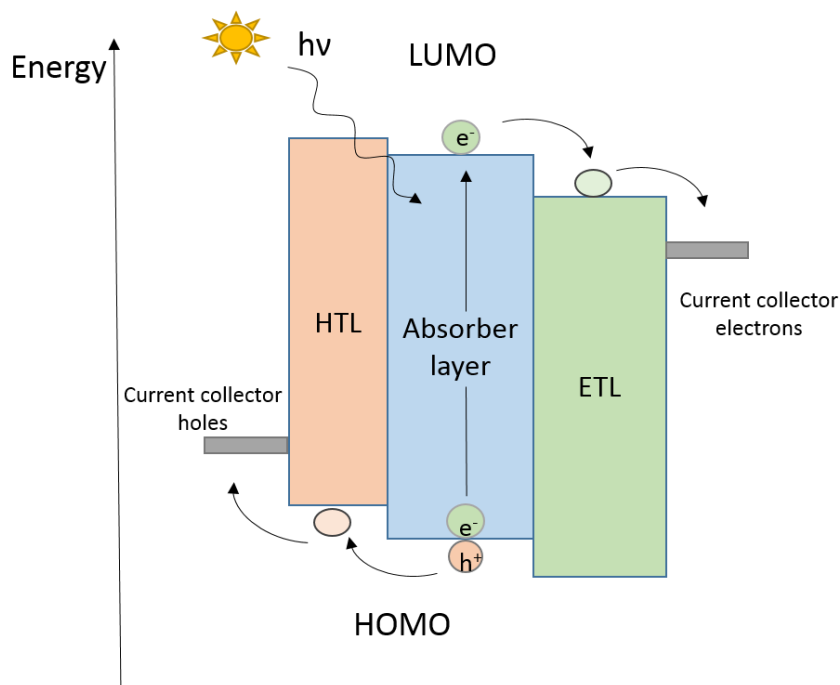


Figure 4: Schematic visualisation of charge carrier transport in organic semiconductors, with electrons (e^-) and holes (h^+) diffusion towards the respective current collectors

This gradient of energy is achieved with materials in very thin films ($<1\mu\text{m}$) close to each other with different energy levels of the highest occupied molecular orbital (HOMO) and the lowest unoccupied molecular orbital (LUMO).⁹ This is analogue to the excitation of an electron from the valence band to the conduction band in inorganic semiconductors. The difference in energy of the two energetic states is called the band gap energy (E_g). The band gap of organic semiconductors also has an influence on the optical absorption spectrum. Lower band gap materials often have a broader spectrum of absorbance. The excitons are separated in their respective free charges by a potential gradient to contacted conducting materials. Since the system tries to minimise its energy, electrons tend to diffuse to materials with a lower energetic LUMO level and holes tend to diffuse in materials with a higher energetic HOMO level. If the work function of the neighbouring material are chosen in a way, that a low work function material is used to transport electrons (electron transport layer = ETL) and a high work function material is used to transport holes (hole transport layer = HTL), the energy gradient can lead to diffusion currents.^{4,8,10,11}

2.1.2 Characterisation of solar cells

Standard solar cell characterisation is done at 25°C under a light source with an illumination power of 100 mW/cm^2 , and a spectrum, that matches the spectrum of the sun at an incident angle of 48.2° , called the AM 1.5 spectrum.^{4,12} One source of the most significant information is the current – voltage measurement (IV–measurement) (Fig. 5), which can be obtained by applying a voltage to the solar cell device and measuring the response current.

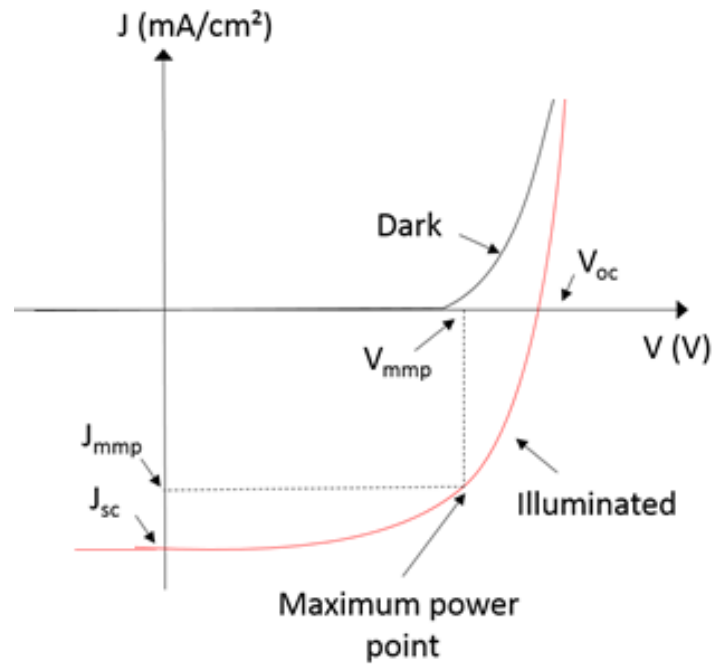


Figure 5: Schematic illustration of a typical IV-measurement

Various interesting characteristics can be derived from the IV – measurement, like open circuit voltage (V_{oc}), short circuit current (I_{sc}), fill factor (FF), maximum power point (mmp), voltage and current at maximum power point (V_{mmp} and I_{mmp} respectively), as well as power conversion efficiency (PCE).

On the point of V_{oc} , no current runs through the external circuit, hence $I = 0$, this is the maximum voltage the solar cell can deliver.¹³ In inorganic semiconductors the V_{oc} is determined by the built-in field, originating from bending of conduction band and valence band^{10,14}, whereas in organic semiconductors the difference in HOMO energy levels of electron donors and the LUMO energy levels of acceptors correlates to open circuit voltage.¹⁵ Furthermore, the V_{oc} is also affected by the morphology of the active absorber layer¹⁶ and the interface between active material and HTL or ETL.^{4,17}

To make solar cells more comparable to each other, the I_{sc} is often replaced by the short circuit current density (J_{sc}), which takes also the surface of the solar cell into account. J_{sc} is given in mA/cm² and it describes the current density that flows through the external circuit when the electrodes of the device are short-circuited, hence $V = 0$. The short circuit current strongly depends on the number of photons that get absorbed and the number of charge carriers that can be excited and extracted. Therefore the maximum J_{sc} is in close correlation with the optical properties of the material such as absorption and reflection.¹³ However not only the possibility

to generate charge carriers by absorption also the charge carrier mobility has influences on the short circuit current.¹⁸

Another point of interest is the maximum power point (MMP), which describes the maximum power that could be harvested from the solar cell. The maximum power point can be obtained by multiplication of voltage and current and determining the maximum of the resulting curve. Voltage and current at the MMP are referred to as V_{mmp} and I_{mmp} respectively. The product of those, defines a rectangle with the largest possible area for any point on the I –V – curve.⁷

With the information of the MMP, one can calculate the fill factor (FF). The FF describes the ratio between the area of the rectangle defined by V_{mmp} and I_{mmp} and the rectangle defined by V_{oc} and I_{sc} , mathematically expressed by formula 1.^{7,13}

$$FF = \frac{V_{mmp} * I_{mmp}}{V_{oc} * I_{sc}} \quad (1)$$

The fill factor describes, to put it simply, the ratio of theoretical possible power that could be extracted from the solar cell, to the actual extracted power. It is affected by the charge carrier transport, internal resistance and charge carrier recombination⁴, thereby FF is always <1, since theoretical maximum is not reached, due to mentioned reasons. The maximum FF is dependent on a lot on the properties of a material, e.g. silicon cells in laboratory and commercial use having maximum FF values of 0.85 and 0.83 respectively, whereas GaAs solar cell are approaching a FF of 0.89.¹³

The most important solar cell characteristic however is the power conversion efficiency η . (PCE). This value describes the conversion of the input power (P_{in}) from the light source, normally 100 mW/cm², to output power measured in the external circuit. (Formula 2)⁷

Explaining the value for FF from formula 1 and expressing the current as current density gives

$$\eta = \frac{P_{out}}{P_{in}} = \frac{V_{mmp} * J_{mmp}}{P_{in}} = \frac{V_{oc} * J_{sc} * FF}{P_{in}} \quad (2)$$

This value is to be considered the most informative, since it describes overall performance of a solar power device.¹³ PCE is dependent on all previous mentioned characteristics and the commercial value of solar cells is partially dependent on the PCE.

2.2 TYPES OF SOLAR CELLS

2.2.1 Silicon solar cells

Solar cells based on silicon were the first to be fabricated in a commercially way with efficiencies of starting 6%.^{13,19} The advantages of using silicon as photoactive absorber material are manifold: it is very abundant, well understood, has a high stability and is non-toxic. Further silicon industry is well adopted and methods are already known to fabricate high purity products. The band gap of silicon is at 1.12 eV, correlating to a absorption onset at 1160 nm.^{20,21} This band gap and absorption values are very close to the values for achieving optimum energy conversion, with the use of a single element semiconductor. The theoretical conversion efficiency limit was calculated to be 33.5% at 25 °C for a semi-infinite thick silicon solar cell.²² The drawback of this is that silicon is an indirect semiconductor, which means valence band maximum and conduction band minimum are not aligned on the same position of the wave vector. Consequently, charge carrier excitation is a three particle process and much more unlikely to happen in contrast to a direct semiconductor, and in addition, recombination energy is mainly converted to heat.^{23,24} So the realistic achievable silicon solar cell efficiency has been calculated to be 29.4%.^{20,25,26} Despite all this, silicon solar cells have achieved nearly their maximum efficiency, due to high ingenuity in terms of process optimisation. With simple wafer texturing, combined with rear surface mirrors and anti-reflection coatings, p-n-junctions made of silicon wafers (~100 – 150 µm) can reach nearly optimal solar cell efficiency.²⁰ The most prevalent material for silicon solar cells is crystalline silicon (c – Si) in different modifications depending on the crystallinity, like monocrystalline silicon, polycrystalline silicon and epitaxial silicon. These are produced in forms of silicon ingots, ribbons or wafers.²¹ Typical device architecture is a p-n-junction with antireflection coating. (Fig. 6)¹³

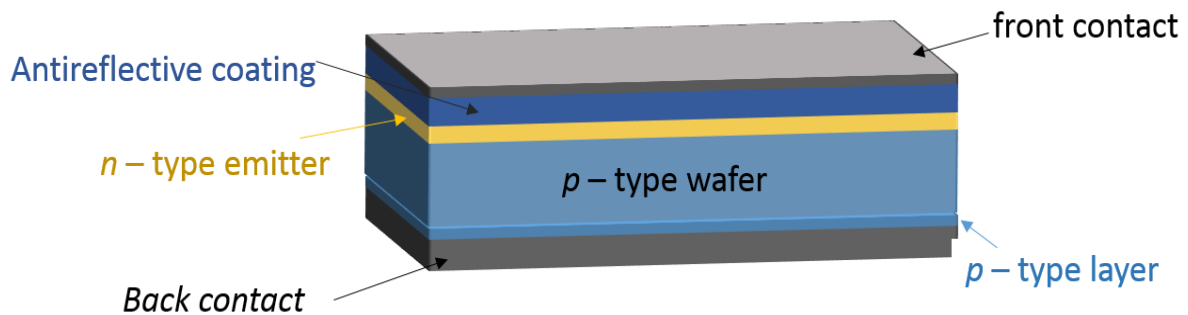


Figure 6: scheme of a modern crystalline silicon cell

Depending on architecture and type of silicon used, different efficiencies are obtained. Overall silicon solar cells have relatively high J_{sc} and FF values. (Tab. 1)²⁷

Table 1: solar cell characteristics of different types of silicon solar cells. Publisher abbreviations: FhG-ISE: Fraunhofer Institut für Solare Energiesysteme, AIST: Japanese National Institute of Advanced Industrial Science and Technology²⁷

Silicon-type	PCE [%]	V_{oc} [mV]	J_{sc} [mA/cm ²]	FF [%]	Publisher
crystalline	26.7 ± 0.5	738	42.65	84.9	Kaneka ²⁸
multicrystalline	21.9 ± 0.4	672	40.76	79.7	FhG-ISE ²⁹
amorphous cell	10.2 ± 0.3	896	16.36	69.8	AIST ³⁰
microcrystalline	11.9 ± 0.3	550	28.72	75.0	AIST ³¹

2.2.2 Thin film solar cells

Another type of solar cell uses thin film semiconductors, thus called “thin film solar cells” (TFSC), with a direct band gap to harvest solar energy. Typical materials are pure semiconductor elements like Germanium (Ge), semiconducting alloys like Cu(InGa)Se₂ (CIGS) and cadmium telluride (CdTe), as well as III-V semiconductors.³² One common material are CIGS, which is a combination of copper indium selenite and copper gallium selenite. Depending on the ratio of Ga to In the band gap of CIGS cells is between 1.03 eV and 1.68 eV.³³ The device setup for CIGS cells is a planar heterojunction where the CIGS material is deposited on molybdenum (Mo) back contact. The p–n–junction is achieved by depositing a thin layer (~50nm) of cadmium sulphide (CdS) on top of the CIGS layer. The device is further composed of a transparent conductive oxide (TCO) (in this case, aluminium doped zinc oxide (AZO)) and a front contact electrode. (Fig. 7) CIGS layers can be deposited via coevaporation of the components or via a two-step deposition, where Cu, In, and Ga are sputter on a substrate and afterwards thermally annealed in Se-vapour. The advantages of CIGS solar cells are their high efficiency and that they can be used in flexible solar devices. On the other hand, CIGS cells are

relatively expensive, due to their use of expensive elements, like gallium and indium, as well as their high production cost. Further it is rather difficult to produce devices with a large area.¹³

Solar cells based on CdTe are one of the most promising solar devices for commercial use, since they offer the lowest cost per watt. CdTe has a band gap of 1.44 eV, which is considered a value close to the optimum for a single junction solar cell. Solar cells are usually composed of a TCO (in this case indium doped tin oxide (ITO)) on a glass substrate. On top of this layer, a thin CdS layer is deposited, followed by the CdTe alloy. Finally, the device is completed with a metal back contact.¹³ (Fig. 7) There are many methods to fabricate CdTe solar cells, like physical vapour deposition, sputter deposition, electro deposition, metal organic chemical vapour deposition, spray deposition, screen print deposition or vapour transport deposition.³⁴ The disadvantages of CdTe solar cells are the toxicity of Cd, although CdTe has been proven less toxic than elemental Cd, and the abundance of Te, due to its low amount in the earth's crust.¹³

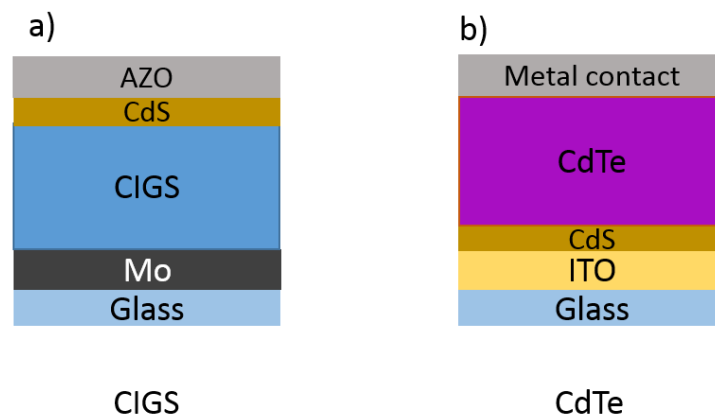


Figure 7: schematic setup of solar cell devices for a) CIGS cells and b) CdTe cells

III–V semiconductors are composed of an element with three valence electrons like Gallium (Ga) or Indium (In) and an element with five valence electrons like Arsenic (As) or Phosphorus (P). Various combinations have been examined like gallium arsenide (GaAs), gallium phosphate (GaP), indium phosphate (InP) or indium arsenide (InAs). Also more complex materials like GaInAs and GaInP are known.¹³ Although remarkable solar cell efficiency can be achieved with III–V semiconductors based on Ga, As and In, these devices have a few downsides. Since gallium is with 14 ppm in the Earth's crust a rather rare element³⁵, thus global coverage of Ga–based solar cells is not possible. Arsenic is highly toxic and it is strongly

suggested that GaAs probably is carcinogenic for humans.³⁶ Furthermore, these elements are all very expensive, due to their low abundance. This limits the use of this highly efficient materials to space use only.¹³ A summary of the solar cell characteristics is given in Tab. 2.

Table 2: solar cell performance of state of the arts thin film solar cells. [state 2017]²⁷

Material	PCE [%]	V _{oc} [mV]	J _{sc} [mA/cm ²]	FF [%]	Publisher
GaAs	28.8 ± 0.9	1122	29.7	86.5	Alta Devices ³⁷
CIGS	21.7 ± 0.5	718	40.7	74.3	Solar Frontier ³⁸
CdTe	21.0 ± 0.4	875	30.3	79.4	First Solar ³⁹

2.2.3 Multi-junction cells

Multi-junction cells are composed of several layers of different optical absorber materials, to achieve a synergetic effect in absorption. Since absorption is limited to a certain wavelength for a certain material, the combination of absorbers with different absorption spectra, therefore different band gap energies, can render a high efficiency solar cell.⁴⁰ This can result in rather complex device architectures, since interlayers have to be introduced to control charge carrier transport, as well as interface problems between the layers. One typical multi-junction device composed of direct semiconductors is a Ge/GaAs/GaInP triple-junction.¹³ (Fig. 8)

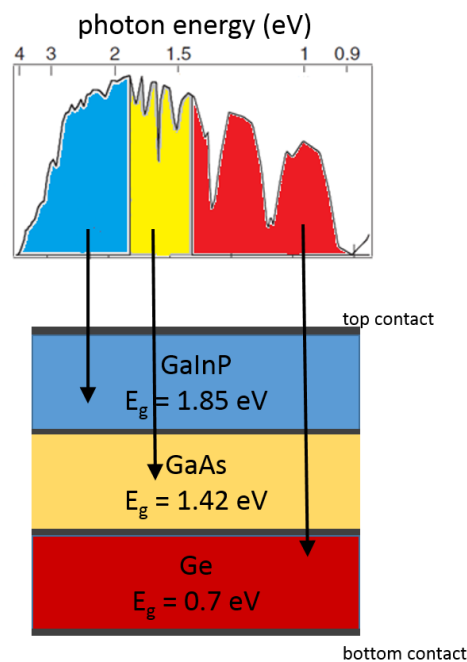


Figure 8: triple-junction solar cell, composed of Ge bottom cell, GaAs as middle cell and GaInP as top cell, with correlating absorbance in the solar spectrum

In this setup, the band gap values are chosen in a matter, that a broad variety of the solar spectrum is absorbed.⁴⁰ This means, considering light enters from the top, that due to low penetration depth of high energetic light, like UV radiation, the highest band gap material functions as top cell so that the most energy is absorbed by it, in this case GaInP. In contrary to this, low energetic light, meaning infrared light, has the highest penetration depth, therefore low band gap materials are placed on the bottom of the device so that higher wavelength radiation is absorbed by all layers.¹³ With this technology at hand, multiple different devices have been manufactured and investigated, up until a five level multi-junction. The most common are based on GaAs, GaInP and GaInAs. These III–V semiconductor multi junction devices, achieve excellent efficiencies.²⁷ (Tab. 3)

Table 3: III – V semiconductor multi – junction device performances²⁷

Device	PCE [%]	V _{oc} [V]	J _{sc} [mA/cm ²]	FF [%]	Publisher
5 junction cell (bonded)	38.8 ± 1.2	4.77	9.56	85.2	Spectrolab ⁴¹
InGaP/GaAs/InGaAs	37.9 ± 1.2	3.10	14.27	86.7	Sharp ⁴²
GaInP/GaAs(monolithic)	31.6 ± 1.5	2.54	14.18	87.7	Alta Devices ⁴³
GaInP/GaInAs/Ge;	34.5 ± 2.0	2.66	13.10	85.6	UNSW/Azur/Trina ⁴⁴

2.2.4 Organic solar cells

Inorganic semiconductors face several obstacles in PV use, since most of the materials are either complex in manufacturing (Si–wafers) or not very abundant and toxic (GaAs). Therefore, an alternative to this materials are organic PV, which offer multiple advantages in comparison to their inorganic counterparts. Organic and polymeric PVs are light weighted, easily processable, offer low material consumption by thin film technology, they can take flexible shapes and have low costs in large-scale industrial production. Furthermore, they are very versatile in their material synthesis and device architecture and offer a broad variety of methods to tune band gap energies. In addition, integrability into other products, such as textiles, papers and foils, can be achieved.⁴⁵

As mentioned in chapter 2.1.1, in organic semiconductors charge carrier separation occurs by diffusion of the separated electrons and holes to their respective conducting layers by an energy level gradient of the LUMO and HOMO levels respectively.⁴ Thus, charge carrier separation is only possible on the interface of a material, which can easily dispatch an electron (donor), and a material that has a high electron affinity (acceptor). Since the exciton only

moves via “hopping” processes from one molecule to the other, compared to direct band transport in inorganic semiconductors, the average exciton diffusion length is far shorter than in inorganic PV materials. Due to the fact that the diffusion length in organic semiconductors is $\sim 10\text{nm}$, these materials are limited to very thin layers.^{46,47} Two main different device structure types have arisen, bilayer and bulk heterojunction. (Fig. 9) In a bilayer structure donor and acceptor material are in planar contact to each other in very thin films. This ensures that nearly all of the separated charges are transported to the current collector, since layer thickness equals the diffusion length. However, charge carrier separation is limited to a small interface. In bulk heterojunction a heterogenic mix of donor and acceptor is formed, this results in a much bigger interface, where charge carrier separation can occur. On the downside, charge carriers might not reach the current collector, since recombination on the interface is much more likely. Furthermore, inclusions of donor material in the acceptor or vice versa, can result in a loss of current, since charges cannot diffuse to their respective electrode.^{13,45}

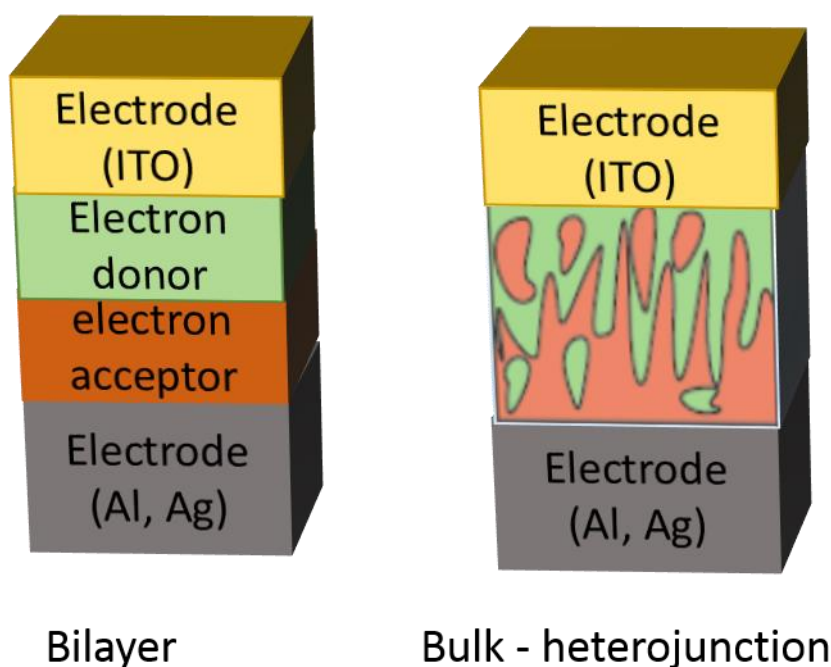


Figure 9: schematic device setup of an organic solar cell in bilayer and bulk heterojunction system.

Given by the nature of the organic components useable in such a device, a broad variety of different donor and acceptor molecules can be used. Only to mention a few, the most common used molecules for a long time were poly-(3-hexylthiophen-2,5-diyl) (P3HT) as an electron donor and [6,6]-phenyl-C₆₁-butyric acid methyl ester (PCBM) as acceptor.(Fig. 10)^{13,48}

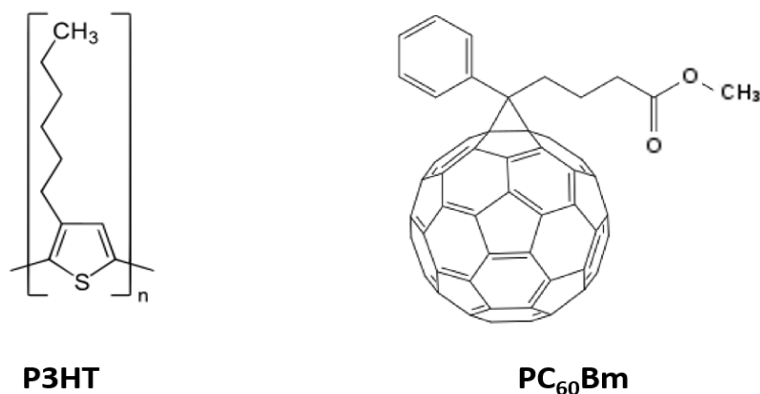


Figure 10: chemical structure of P3HT and PCBM

As manifold as the possible organic molecules are, as manifold are the different device performances. Overall one can say that most organic system were in the range of an efficiency below ~10% since development, just recently organic photovoltaics cracked the 10% mark.²⁷(Tab. 4)

Table 4: best efficiency of organic solar cell [state:2017]²⁷

	PCE [%]	V _{oc} [mV]	J _{sc} [mA/cm ²]	FF [%]	Publisher
Organic cell	11.2 ± 0.3	780	19.30	74.2	Toshiba ⁴⁹

2.2.5 Dye sensitized solar cell

The DSSC was originally invented by O'Regan and Grätzel⁵⁰ in 1991, therefore they are also called Grätzel cell, and has seen a lot of interest since then. The principle in this setup is that a sensitizer dye (S), usually a ruthenium complex, which is put into an excited state (S*) upon photon radiation, can transfer electrons into a mesoporous titanium dioxide (TiO₂) layer. This is possible, because the energy level of S* is higher than the conduction band of TiO₂. Electrons then diffuse through the TiO₂ to a transparent conductive oxide, mostly ITO, fluorine doped tin oxide (FTO) or AZO. The dye, which is now positively charged, regenerates its charge neutrality via a redox reaction with iodine (I⁻)-ions in a liquid electrolyte. I⁻ is further oxidised with I₂ to I₃⁻ and diffuses towards the counter electrode (usually platinum (Pt)), where it is regenerated to I⁻ with energy from the external circuit.^{13,51,52} (Fig.11)

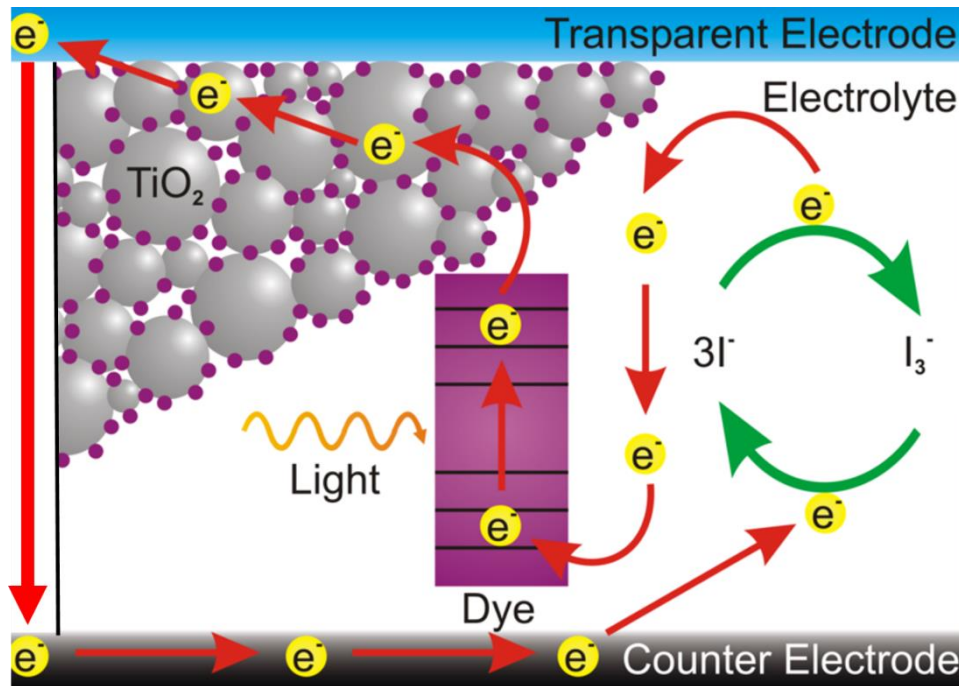


Figure 11: schematic function principle of a dye sensitised solar cell. Original work by M. R. Jones⁵³

DSSC offer average efficiencies and are a competitive PV type to silicon solar cells in terms of efficiency-price-ratio.²⁷ The major advantage of DSSC is that due to the monolayer of dye material electron diffusion only takes place in TiO₂. Due to this favourable differential kinetics DSSCs work even under low light conditions, which means cloudy sky and indirect illumination, whereas other systems tend to lose a major part of their efficiency.⁵⁴ On the other hand, the use of a liquid electrolyte comes with other problems. The electrolyte can freeze under low temperatures or expand upon heating and therefore damage the device or stop power generation.⁵⁵ One solution to this problem is the use of solid-state electrolytes, which are researched by multiple working groups to find appropriate materials.

Table 5: best performance of a DSSC [state: 2017]²⁷

	PCE [%]	V _{oc} [mV]	J _{sc} [mA/cm ²]	FF [%]	Publisher
Dye sensitized solar cell	11.9 ± 0.4	744	22.47	71.2	Sharp ⁵⁶

2.2.6 Perovskite solar cells

Perovskite solar cells (PSC) are one of the youngest field of solar cell research, but also the fastest growing. Only within a few years from starting less than 4% PCE in 2009 to now confirmed above 22% in 2014.⁵⁷ PSCs use a perovskite material, which has an ABX_3 structure, as optical absorber. The name is originating from the structure of the mineral perovskite, which actually is calcium titan oxide ($CaTiO_3$), however mainly halogenates are used for solar cell applications. B represents a divalent cation, in most common cases lead (Pb^{2+}), tin (Sn^{2+}), germanium (Ge^{2+}) or antimony (Sb^{2+}), which is cantered at an octahedron of X atoms. X represents a monovalent halide anion, such as chloride (Cl^-), bromide (Br^-) or iodide (I^-). A represents a monovalent cation, which can on the case of inorganic–organic hybrid perovskites, also be an organic component with a positive charged side group. The A cation occupies the inter lattice space between the formed octahedrons. (Fig. 12)

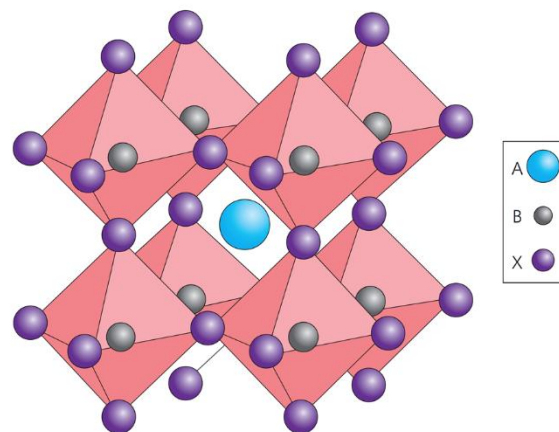


Figure 12: schematic perovskite structure, with A= monovalent cation, B= divalent cation and X= monovalent halide anion⁵⁸

The perovskite material acts as an optical direct band gap semiconductor. Excited electrons are harvested via diffusion processes, based on the same principle as in organic solar cell devices, by an energetic gradient, induced by a HTL and an ETL. The usual setup of a perovskite solar cell can roughly be described by two different systems: a n–i–p junction, and a p–i–n junction. In n–i–p systems, device architecture is similar to those of a DSSC, where the perovskite is infiltrating a mesoporous network of TiO_2 . On top of the absorbing layer a p – type material, like P3HT or *N,N,N',N',N'',N'',N''',N'''*-Octakis(4-methoxyphenyl)-9,9'-spirobi[fluorene]-2,2',7,7'-tetramine (Spiro-MeOTAD), is used as HTL. Also planar n–i–p junctions exist, in which the mesoporous TiO_2 is replaced by another n–type material, like zinc oxide (ZnO) or just planar TiO_2 . On the contrary, p–i–n junctions are built in an inverted setup,

where the absorbing layer is deposited on a p-type material, like nickel oxide (NiO) or poly(3,4-ethylenedioxythiophene):polystyrene sulfonate (PEDOT:PSS). In this case, the ETL is composed of n-type materials, often PCBM, or C₆₀ Buckminster fullerenes. All device setups use a TCO and gold (Au), silver (Ag) or aluminium (Al) as electrode materials.^{59,60} (Fig. 13)

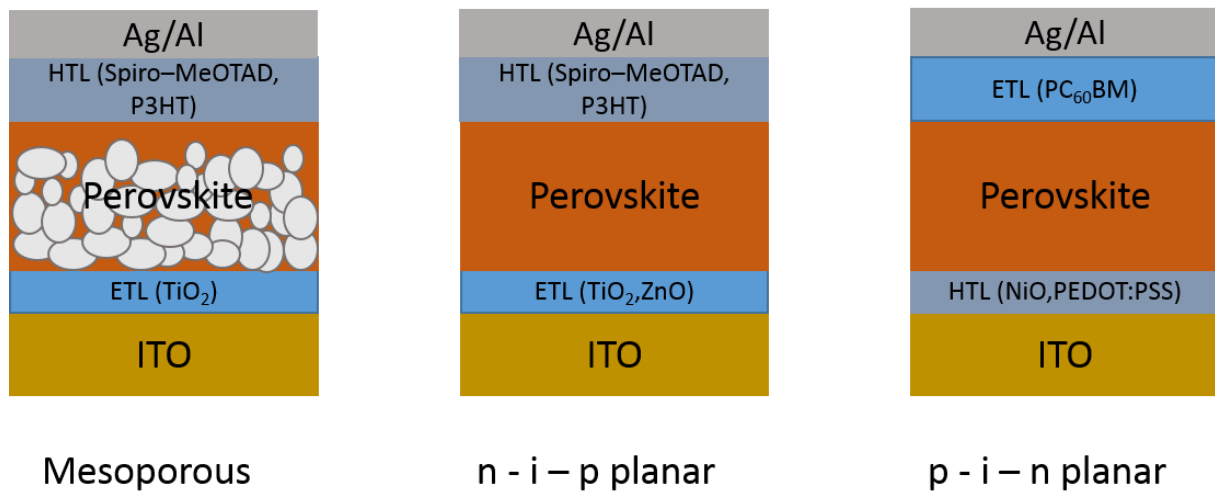


Figure 13: schematic device setup of a perovskite solar cell. HTM= hole transport material ETM= electron transport material

PSCs have many advantages, like high absorption coefficients, easily tuneable band gaps, high charge carrier mobility, a balanced electron and hole transport, and long carrier diffusion lengths.^{61,62} Another important feature of PSCs is that they are easily processable with various techniques, like solution-based spin coating and evaporation methods. Downsides are their low stability to air and moisture as well as the toxicity of lead-based devices.^{59,63}

Since this work focuses on perovskite solar cells, a more detailed description of the different types of perovskite solar cells is given in the following chapters.

2.3 GENERAL OVERVIEW OF PEROVSKITE SOLAR CELLS

2.3.1 Lead based perovskite solar cells

The most extensively investigated and highest efficient perovskite cells are based on Pb as B-side cation. The most common used halide for lead perovskites is iodine, although bromide and chloride are also used in small amounts to tune the optical band gap. The A side cation can either be inorganic, namely caesium (Cs⁺) or rubidium (Rb⁺), or organic, where mainly methyl ammonium (CH₃NH₃⁺, MA⁺) and formamidinium (CH(NH₂)₂⁺, FA⁺) are used.^{59,63}

The energetic properties of perovskite absorber layers can easily be tuned by changing the content and sort of the halide side X in MAPbX₃ perovskites (X=Cl, Br, I).⁶⁴ By changing the halogen from I, to Br to Cl the band gap decreases respectively.⁵⁹ Theoretical reports have given rise to ideas to fabricate mixed halide perovskites, indicating suggestion that an I, Cl mixed perovskite is hard to form with an high content of Cl, whereas combinations of I, Br and Br, Cl are relatively easy to produce.^{65,66} The work of Seok et. al.⁶² first demonstrated a tuning of the band gap from 1.6 – 2.2 eV, by changing the bromide content in mixed halide perovskite MAPbI_{3-x}Br_x. This offers a lot of potential for the use of different mixed halide perovskites in multi cell systems (tandem cells).

Furthermore lead based PSC have high efficiency values up to 22% and, since they can be produced by a broad variety of different methods and in different setups, are a very attractive material for large-scale solar cell production. Therefore, it is no surprise that PSC have drawn so much attention and the research was making fast progress in the last 5 years. However, some obstacles are yet to overcome before the commercialised use of PSCs.⁵⁹ The major problem lies in the stability of the perovskite material, especially over a long term. Although not all intrinsic and extrinsic factors contributing to perovskite stability are fully investigated, two critical factors for perovskite lifetimes are known to be problematic, namely moisture sensitivity and thermal stability.⁶⁷ Several experiments focused on the increase of moisture resistance, both by improvement in sealing the device from air moisture⁶⁸ and changing perovskite properties to achieve higher moisture resistance, by the formation of an (PEA)₂(MA)₂[Pb₃I₁₀] (PEA = phenethyl ammonium, C₆H₅(CH₂)₂NH₃⁺) perovskite.⁶⁹

2.3.2 Lead – free perovskite solar cells

PSC based on lead, suffer from a major environmental problem, due to the toxicity, carcinogenicity and bioavailability of lead and lead halides, as well as the water solubility of lead, which might contaminate the soil and water supplies.^{63,70,71} Therefore, a need for a non-toxic, environment-friendly perovskite absorber has arisen.⁷² Since the perovskite structure allows for many combinations of used elements and molecules, a broad variety of different materials has been investigated by a lot of working groups.⁶³ The substitution of lead with a nontoxic element can be achieved via two different methods. First, homovalent substitution with isovalent cations from group-14 elements (Sn, Ge), alkaline earth metals (calcium (Ca),

strontium (Sr), barium (Ba)), transition metals (manganese (Mn), iron (Fe), nickel (Ni), copper (Cu), palladium (Pd)) and lanthanides (europium (Eu), ytterbium (Yb)). Secondly, heterovalent substitution by aliovalent metal cations, like main group elements (thallium (Tl), bismuth (Bi), antimony (Sb), tellurium (Te)) and lanthanides and actinides. Due to the need of charge neutrality in the ABX_3 structure, direct substitution is not possible. However, substitution can be accomplished by the use of mixed-valence cations, where an equal proportion of mono- and trivalent cations can give an overall divalent state.^{63,73}

Since the possible materials are so manifold and investigation in detail has already been reported several times^{63,74,75} only a short overview of selected perovskite types will be presented in this work. This chapter focuses on the performance and properties of PSC devices based on Ge, Sb, and Bi. In addition, the work on Sn-based PSC will be described in more detail in the following chapter, due to the focus in Sn-perovskites in this work.

2.3.2.1 Germanium perovskite solar cells

One natural candidate for substituting lead is germanium, due to its semiconducting behaviour and its favourable oxidation state. Compared to Pb^{2+} , Ge^{2+} has a lower electronegativity, a smaller ionic radius and a more covalent character.^{76,77} Although a promising candidate for substitution, Ge-based perovskites suffer even more from the problem of stability as Sn or Pb due to the instability of the Ge^{2+} -ion.⁷⁸ This might one reason why research groups have only rarely investigated germanium perovskites. However, different perovskite materials of the type $AGeI_3$ (A= Cs, MA, FA) have been characterised, to get a basic understanding of their properties. In terms of band gap tuning, experimental data shows that the band gap increases from a small cation, like Cs^+ ($E_g = 1.6$ eV) to bigger cations like MA^+ ($E_g = 1.9$ eV) and FA^+ ($E_g = 2.2$ eV).⁷⁹ Ge-perovskites with Cs^+ and MA^+ have been used in the DSSC type of PSCs yielding PCE values of 0.11% and 0.20%, respectively. (Tab.5)⁸⁰

Table 6: Ge – perovskite solar cell performance⁸⁰

Material	PCE [%]	V_{oc} [mV]	J_{sc} [mA/cm ²]	FF [%]
CsGeI ₃	0.11	74	5.7	27
MAGeI ₃	0.2	150	4	30

The relatively low performance of Ge-based perovskites is mainly, due to the instability and the high defect concentration coming with it.⁸¹ Nonetheless, germanium perovskites are a

promising material for solar cell applications and there is much room for improvement, since the full potential of this perovskite type is by far not exploited.⁶³

2.3.2.2 Antimony perovskite solar cells

Antimony is a potential candidate for heterovalent substitution due to the fact that Sb^{3+} is isoelectronic to Sn^{2+} and has a comparable electronegativity.⁸² Contrary to other perovskites, Sb-based materials have, due to the difference in oxidation state, the structure $\text{A}_3\text{Sb}_2\text{X}_9$ (X = Cl, Br, I) with A being an organic (NH_4^+ , MA^+ , FA^+) or an inorganic (Cs^+ , Rb^+) cation. As with other perovskites, band gap energy depends on the character of X and A, whereas values for Sb – based perovskites are relatively high reaching from 1.89 eV, for $\text{Cs}_3\text{Sb}_2\text{I}_9$ to 2.48 eV for $\text{Rb}_3\text{Sb}_2\text{Br}_9$.⁶³ similar to germanium based materials, not much experimental data is available for Sb–perovskites in solar cell applications. Two of the most promising experiments were carried out by Hebig et al. using a planar inverted device setup (ITO/PEDOT:PSS/ $\text{MA}_3\text{Sb}_2\text{I}_9$ /PC₆₀BM/ZnO-NP/Al)⁸³ and Harikesh et al. utilising a DSSC architecture (FTO/c-TiO₂/mp-TiO₂/ $\text{Rb}_3\text{Sb}_2\text{I}_9$ /poly-TPD/Au) (poly-TPD= poly[*N,N*-bis(4-butylphenyl)-*N,N*-bisphenylbenzidine]).(Tab. 6)⁸⁴

Table 7: most promising solar cell performance for Sb – based PSCs⁶³

Material	PCE [%]	V _{oc} [mV]	J _{sc} [mA/cm ²]	FF [%]
$\text{MA}_3\text{Sb}_2\text{I}_9$	0.5	890	1.1	55
$\text{Rb}_3\text{Sb}_2\text{I}_9$	0.66	550	2.12	57

Overall antimony perovskites suffer from a relatively low J_{sc} , which is partially originated in high band gap values. However, Sb–perovskites need a lot more research on their PV applications, since similar to Ge – perovskites the full potential of this material is yet to be discovered.

2.3.2.3 Bismuth perovskite solar cells

Like antimony, Bi–based perovskites are one possibility of heterovalent substitution of lead, since Bi^{3+} -ions are isoelectric to Pb^{2+} -ions. The most intensively studied species of Bi-perovskites is $\text{MA}_3\text{Bi}_2\text{I}_9$, which is an environment friendly and rather air and moisture stable semiconductor.⁸⁵ $\text{MA}_3\text{Bi}_2\text{I}_9$ has a rather high band gap of 2.10 eV⁸⁶ and a high exciton binding energy⁸⁷, which limits exciton generation and charge carrier separation, thus overall limiting photovoltaic performance by low J_{sc} values.⁶³ Solar cells in planar inverted

(ITO/PEDOT:PSS/MA₃Bi₂I₉/PCBM/Ca/Al) and planar heterojunction cells (FTO/TiO₂/mp-TiO₂/MA₃Bi₂I₉/ Spiro-OMeTAD/MoO₃/Ag) architecture have been fabricated by Ötz et al. and Zhang et al., respectively.^{85,88} Further Park et al published a Bi-based perovskite with Cs⁺ in a mesoporous setup (FTO/c-TiO₂/mp-TiO₂/ Cs₃Bi₂I₉/Spiro-OMeDAT/Ag) with record efficiency of 1.09 %⁸⁹

Table 8: performance of MA₃Bi₂I₉ and Cs₃Bi₂I₉ PSCs in different device setups⁶³

Setup	PCE [%]	V _{oc} [mV]	J _{sc} [mA/cm ²]	FF [%]
MA ₃ Bi ₂ I ₉ planar inverted	0.1	660	0.22	49
MA ₃ Bi ₂ I ₉ mesoporous	0.42	670	1.0	62.5
Cs ₃ Bi ₂ I ₉ mesoporous	1.09	850	2.15	60.0

2.4 TIN-BASED PEROVSKITE SOLAR CELLS

2.4.1 State of the Arts research on Sn-perovskites

Perovskites based on Sn as substitution for Pb, came as soon as the problems of Pb – based devices raised. The most common Sn-perovskites are of the form ASnI₃ (A = Cs, MA, FA), which have been investigated in close detail. CsSnI₃, MASnI₃ and FASnI₃ are direct band gap semiconductors with an E_g of 1.3 eV, 1.26 eV and 1.42 eV, respectively.^{90,91} Thus resulting in a broad absorption over nearly the whole spectrum of the sun, making them ideal materials for PSCs.

These perovskite solar cells are usually fabricated via solution based processes like spin coating or doctor blading, and various different devices based on mesoporous or planar TiO₂ heterojunctions or planar inverted setups exist.^{63,92} Devices utilising compact and/or mesoporous TiO₂ as ETL, normally use Spiro-MeOTAD as HTL, although some devices with poly (triaryl amine) (PTAA) as HTL exist.^{74,93} As for inverted structures, the most common HTL materials are PEDOT:PSS and NiO in combination with PC₆₀BM or a C₆₀/bathocuproine (BCP) as ETL. As Electrode materials a TCO, like ITO or FTO, is used on the transparent electrode side and Ag or Al are used as back contact. Normally all these layers are deposited via solution based methods or evaporation techniques.⁹²

Sn-perovskites are rather sensitive to defects in crystal structure or interface defects. The main problem is the oxidation reaction from Sn²⁺ to Sn⁴⁺, which can add an extra two electrons

to the crystal, hence *n*-dope the material, favouring recombination. Furthermore, Sn^{2+} can easily be lost, by oxidation during spin coating or thermal evaporation, because of its vapour pressure, and therefore change the electrical properties of the material. It is suggested that small amounts of oxidised Sn^{4+} are present in the perovskite structure, even under glovebox condition with water and oxygen concentrations below 1 ppm. Tin has, in terms of ionic stability, rather peculiar properties. E.g.: it is hard to get thermodynamically stable compounds of Pb^{4+} or Ge^{2+} , but since Sn is in the middle of these elements in the 14th group of the periodic table, both Sn^{2+} and Sn^{4+} can form equally probable stable compounds.⁹² As a consequence, Sn-perovskites suffer from pinholes and defects more likely than Pb-based materials. Chung et al. came up with the idea to stabilise Sn-perovskites with tin (II) fluoride (SnF_2),⁹⁴ which was later adopted by Kumar et al., who dedicated a paper to the effects of SnF_2 in CsSnI_3 perovskites on mesoporous TiO_2 . Their work proved that SnF_2 is not directly incorporated in the perovskite crystal structure, hence not disturbing crystallographic properties. Further they stated that 20 mol% SnF_2 was the best amount of to use.^{92,95} Another method to improve control of crystallization was the use of an anti-solvent quenching method, where during spin coating, a solvent, in which the perovskite was not soluble, was dropped onto the substrate to force the material to crystallise. Kim et al. first used this method utilising toluene as anti-solvent.⁹⁶

A factor that has also shown to be crucial for solar cell performance is the purity of utilised tin (II) iodide (SnI_2). Reported experiments state that commercial available SnI_2 contains SnI_4 impurities⁷⁴, and also the degree of purity seems critical. A purity of 99% rendered no functional devices, whereas 99.999% purity of SnI_2 caused wettability problems in precursors, which resulted in fluctuations of efficiency.^{95,97} A purity of 99.99% seemed to be optimal, with respect to solar cell performance. This should rise awareness for the source of used SnI_2 in Sn-perovskite solar cells.⁹²

From the start on, the main device setup researchers used for Sn-based PSC was the DSSC architecture, with planar and mesoporous TiO_2 . Various different combinations of techniques were investigated. To conclude, the best solar cell performances of devices based on DSSC architecture are listed in Tab. 8.

Table 9: PV performance of best Sn–perovskite solar cells build with DSSC device setup⁹²

Perovskite	PCE [%]	V _{oc} [mV]	J _{sc} [mA/cm ²]	FF [%]
MASnI ₃ ⁹⁸	6.4	880	16.8	42
CsSnI ₃ ⁹⁵	2.0	240	22.7	37
FASnI ₃ ⁹⁹	5.3	380	23.1	60

However, as Sn–perovskite research proceeded, more and more attention was drawn by an inverted device setup. High efficiencies were obtained using PEDOT:PSS or NiO as HTL and PC₆₀BM or C₆₀ as ETL.⁹² Liao et al. made a significant step forward by obtaining a 6.2% PCE, with a FASnI₃ PSC. The implemented a mixed solvent precursor, where they used a 4:1 (v/v) mixture of *N,N*–dimethyl formamide (DMF)/dimethyl sulfoxide (DMSO), instead of pure DMF. Further, they decreased the used amount of SnF₂ to 10 mol% and used diethyl ether as anti – solvent.¹⁰⁰ The topmost efficiency was reached with a mixed cation approach by Zhao et al. using an inverted setup and a MA_{1-x}FA_xSnI₃ perovskite.¹⁰¹ The best ratio of the cation combination of MA_{0.75}FA_{0.25}SnI₃ rendered an astonishing efficiency of 8.12%. Top solar cell performance of Sn–perovskite solar cells using inverted setups are listed in Tab. 9.

Table 10: PV performance of best Sn–perovskite solar cells build with inverted device setup⁹²

Perovskite	PCE [%]	V _{oc} [mV]	J _{sc} [mA/cm ²]	FF [%]
MASnI ₃ ¹⁰²	3.2	600	17.8	30
CsSnI ₃ ¹⁰³	3.0	520	9.5	61
FASnI ₃ ¹⁰⁰	6.2	470	22.1	60
MA _{0.75} FA _{0.25} SnI ₃ ¹⁰¹	8.12	610	21.2	62.7

2.4.2 Introduction of PEA⁺ and its role in 2D perovskite formation

Another important step towards increasing efficiency and stability of Sn–based perovskites was the introduction of PEA⁺-cation in the perovskite structure. In analogy to Pb–cells, where a 2D structure is more stable than a 3D structure,¹⁰⁴ a 2D Sn–perovskite was implemented with the use of PEA⁺ as a more bulky organic component. Liao et al. stated the formation of a 2D perovskite on a NiO substrate. The structure was composed of a crystalline perovskite phase with phases of structured bilayers of organic PEA⁺ residues, perpendicular to the surface. (Fig. 14) They substituted the cation of an FASnI₃ with PEA⁺ to obtain an PEA_xFA_{1-x}SnI₃ perovskite, with the result that 20 mol% substitution was the best rendering a PCE of 5.94%, which was stable for more than 100 h.¹⁰⁵ Shao et al. demonstrated even better solar cell

performance using an inverted device setup, utilising only small amounts of PEA⁺ in their devices. They stated that the best amount was 8 mol% for a FASnI₃ based perovskite, reaching top efficiencies of 9%¹⁰⁶

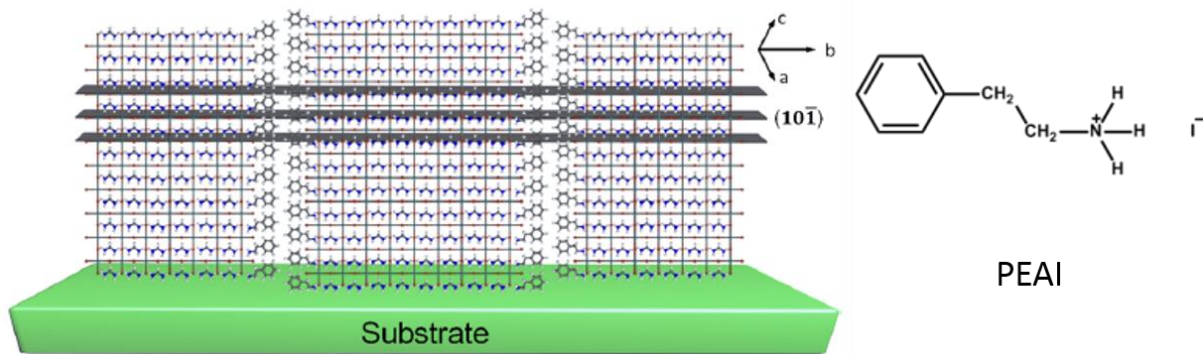


Figure 14: Schematic illustration of 2D structured PEA_{0.2}FA_{0.8}SnI₃ perovskite on NiO substrate¹⁰⁵ and chemical structure of PEA¹⁰⁶

2.4.3 Aim of this thesis

Sn-based perovskites have drawn a lot of attention in the last years to PSC community and have made big advances in the last 5 years from starting below 3 % in 2012⁹² up to 6.2 % in late 2016¹⁰⁰ to now 9 % in mid 2017.¹⁰⁶ Tin perovskites are a field of research, which is fast growing and very promising to bring forth commercially available, non-toxic, environment-friendly and efficient solar devices. This work focuses on the investigation of new Sn-based perovskite for use in solar cell applications. Different amounts and combinations of cations in ASnI₃ perovskites should be investigated to get information on promising new materials. Since inverted device setups have stepped more in the centre of PSC research, a classic setup (ITO/PEDOT:PSS/perovskite/PC₆₀BM/Al) is used to manufacture Sn-based PSC. In addition, the promising change in properties by introducing PEA⁺ into perovskite structure has to be closer examined and tested in multiple different solar devices. The primary goal is to get a deeper understanding how perovskites properties and solar cell performance change, by changing their cation composition, even using multiple cations, and using PEA⁺ in different systems. A very promising aspect, which will be focused on in this work, is the combination of high efficiency mixed cation MA_{0.75}FA_{0.25}SnI₃ with high stable PEA_{0.2}FA_{0.8}SnI₃. This should investigate the possibility of obtaining a high efficient and long term stable Sn – based perovskite device with multiple cations.

3 EXPERIMENTAL

3.1 CHEMICALS

FAI, MAI, and PEAI were purchased from Dyesol. SnI₂ was obtained from Alfa Aesa in 99.999% purity and from Sigma Aldrich in 99.999% purity. SnI₂ was used as purchased, purified as described in chapter 3.2 as well as synthesized after the route described in chapter 3.3. Sn powder (99.8% purity) and iodine (99.5% purity) for the synthesis of SnI₂ were purchased from Sigma Aldrich and abcr, respectively. PEDOT: PSS Clevios P VP.AI 4083 was obtained from Heraeus. PC₆₀BM was purchased from Solenne in 99% purity. DMF, DMSO and chlorobenzene were purchased from Sigma Aldrich in p.a. purity grade. Besides, of SnI₂ all chemical were used as received.

3.2 PURIFICATION OF PURCHASED SnI₂

Purchased SnI₂ was purified using a sublimation technique. Approximately 500 mg of purchased SnI₂ was put in a boat shaped crucible and inserted in a tube furnace. The glass tube was floated with a nitrogen stream and the following temperature program was used: heating up to 480 °C with a heating rate of 20 °C/min, holding temperature for 1h, cooling to room temperature in 2h. Afterwards, the tube was sealed airtight and put in a nitrogen-filled glovebox. The purified SnI₂ was obtained as dark red powder or shards, which had to be scratched out carefully of the crucible. Yellow SnI₄ contaminations resublime at the end of the glass tube. The yield of pure SnI₂ was 80% and 65% from chemicals purchased from Sigma Aldrich and Alfa Aesa, respectively.

3.3 SYNTHESIS OF SnI₂

The synthesis of SnI₂ was adapted and modified from the synthesis route published by Stoumpos et al.⁹⁰

In a 250 ml 3-neck round bottom flask equipped with condenser and gas faucet, 3.6 g of tin powder were dissolved in 40 ml of 2 M aqueous degassed hydrochloric acid (HCl). The apparatus was kept under N₂ gas flow the whole time. 5 g of iodine shards were added via a powder funnel in two portions. Nitrogen flow was reduced at this point to prevent developing

I₂ fumes to crystalize in the condenser. The solution turns dark brown after adding of I₂. The flask was put on a silicon oil bath at 170 °C and stirred for half an hour. As the reaction proceeded, the solution changed its colour to red and finally yellow. Afterwards, the gas stream was slightly increased and tin powder was added in portions of approximately 0.1 g every 10 min. This was to reduce any trace of I₂ and completely reduce present SnI₄ to SnI₂. The reaction was considered complete when the solution has turned bright yellow and tin powder started to precipitate and accumulate to granules. Then the mixture was transferred via decantation into a 100 ml 2-neck flask, equipped with a gas faucet and flushed with N₂ gas. The mixture is immediately immersed in a preheated 170 °C silicon oil bath. After 1 min heating is turned off and the reaction was cooled down from 170 °C to room temperature overnight still immersed in the cooling oil bath. SnI₂ crystallizes as long red needles. The surplus solution was decanted and the product was washed carefully several times with degassed 0.01 M aqueous HCl. Subsequently, the product was dried over vacuum at 70 °C for 5h. Finally, the product was obtained as red needles in a 52 % yield and transferred in the evacuated flask into a nitrogen-filled glovebox for use in precursor solutions.

3.4 PRECURSOR SOLUTIONS

All solution preparation steps were done under nitrogen atmosphere in an MBraun glovebox. Single cation precursors were prepared by dissolving SnI₂ in DMF/DMSO (ratio 4:1 v/v), to obtain a 1M solution. The solution was stirred for half an hour at room temperature. Afterwards, the solution was transferred into a vial with 10 mol% of SnF₂ powder and again stirred for half an hour under room temperature. Subsequently, the precursor was poured onto CsI, FAI, or MAI powder to obtain a 1:1 molar solution. Finally, the precursor solution was stirred overnight. All precursors were filtered through a 0.45 µm PTFE filter right before use.

For precursor with multiple cations, solutions were prepared as mentioned above, with the cation powders mixed in a manner to obtain a 1 M cation concentration with 20 mol% additives.

3.5 DEVICE FABRICATION

For solar cell fabrication, 1.5 x 1.5 cm ITO-coated glass substrates (Resistance: 15 Ω , purchased from Luminescence technology Corp.) were carefully rinsed with acetone and put in a bath of isopropanol. The bath was put under ultrasonic treatment for 30 min at 40 °C. Subsequently the substrates were dried under N₂ gas stream and treated with oxygen plasma for 3 min.

PEDOT:PSS was spin-coated at 3000 rpm for 30s on these substrates and were then put into a nitrogen filled glovebox immediately after, for heat treatment at 120 °C for 20 min.

Perovskite precursor solution was spin coated under glovebox atmosphere with 5000 rpm, and an acceleration of 2000 rpm/s, for 60s. After 20s of spin coating, 50 μ l toluene was dropped onto the substrate from a distance of approximately 5 cm, which changed colour from yellow to grey/black. Afterwards the perovskite was annealed at 70 °C for 10 min. PC₆₀BM (10 mg/ml) was spin coated onto the perovskite layer with 2000 rpm, an acceleration of 1000 rpm/s for 60s. Al – electrode were thermally evaporated in a MB-EVAP in-glovebox thermal evaporator, utilising a SQM – 160 rate/thickness monitor from Inficon, at a rate of 2-6 $\text{\AA}/\text{s}$ and a pressure of $1 \cdot 10^{-5}$ mbar with substrate rotation to a layer thickness of 100 nm. The electrodes were deposited over a mask to obtain six solar cell spots per substrate with an area of 0.09 cm² each.

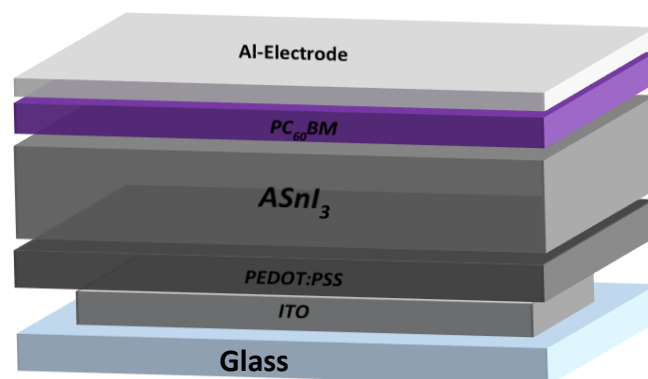


Figure 15: Schematic architecture of one solar cell

For UV/VIS measurements, glass substrates were cleaned the same way as ITO substrates and spin coated with a perovskite precursor solution and annealed, using the same parameters as for the preparation of solar cells. The substrates were taken out of the glovebox after annealing and were measured immediately.

For XRD measurement, glass substrates were cleaned as described above and a precursor solution was spin coated on top, with a speed of 2000 rpm, acceleration of 500 rpm/s for 60s. 80 μ l of toluene was dropped onto the spinning substrate 20s after start. The perovskite layers were annealed as mentioned before. Afterwards a protective layer of poly(methyl methacrylate) (PMMA) (obtained from Sigma Aldrich) 20 mg/ml in chlorobenzene was added via spin coating, at 1000 rpm with an acceleration of 500 rpm/s for 30s. Sample substrates were then sealed under nitrogen atmosphere and send to XRD.

3.6 MEASUREMENTS AND CHARACTERISATION

IV-measurements were recorded using a dedolight 400 D lamp at a light intensity of 100 mW/cm² and a Keithley 2400 source meter. The measurement was done in a voltage range from -1 V to + 1 V, with a delay of 100 ms before each data point, a maximum compliance of 100 mA and a scan rate of 200 mV/s. Also light intensity was measured during measurement.

UV/VIS spectra were measured with a Perkin Elmer Lambda 35 UV/VIS spectrometer, equipped with an integrating Ulbricht sphere, from a range of 400 nm to 1000 nm. Slit width was set to 1 nm and one data point was obtained every 1 nm, with a scan rate of 480 nm/min. A labsphere certified reflection standard was used for absorption and transmission measurements.

Layer thickness measurement were performed with a Bruker DektakXT profilometer with 12.5 μ m radius stylus. The data acquisition was performed with a scanning speed of 100 μ m/s for 10s and a stylus force of 3 mg.

X-ray diffraction measurements were conducted on a PANalytical Empyrean diffractometer in Bragg-Brentano configuration operated at 40 kV and 40 mA using Cu K α radiation ($\lambda = 1.5418$ Å). Measurements were carried out by the Birgit Kunert from the institute of solid-state physics.

The external quantum efficiency (EQE) spectra were measured using monochromatic light from a MuLTImode4 monochromator (AMKO) equipped with a Xenon lamp chopped at 30 Hz. The signals (wavelength increment: 10 nm) were measured by a lock-in amplifier from Stanford Research Systems (Model SR830). A spectrally calibrated 818-UV/DB photodiode (Newport Corporation) was used as a reference.

4 RESULTS AND DISCUSSION

4.1 SINGLE CATION SN-PEROVSKITES

In terms of single cation tin perovskites, three already reported materials (CsSnI_3 , MASnI_3 and FASnI_3) were investigated with regard to their optical and crystallographic properties, as well as their solar cell efficiency to compare the described device setup to already known methods and to get reference values for further experiments.

4.1.1 Optical characterisation

Optical properties of single cation perovskites (CsSnI_3 , MASnI_3 and FASnI_3) were derived from UV/Vis spectra.

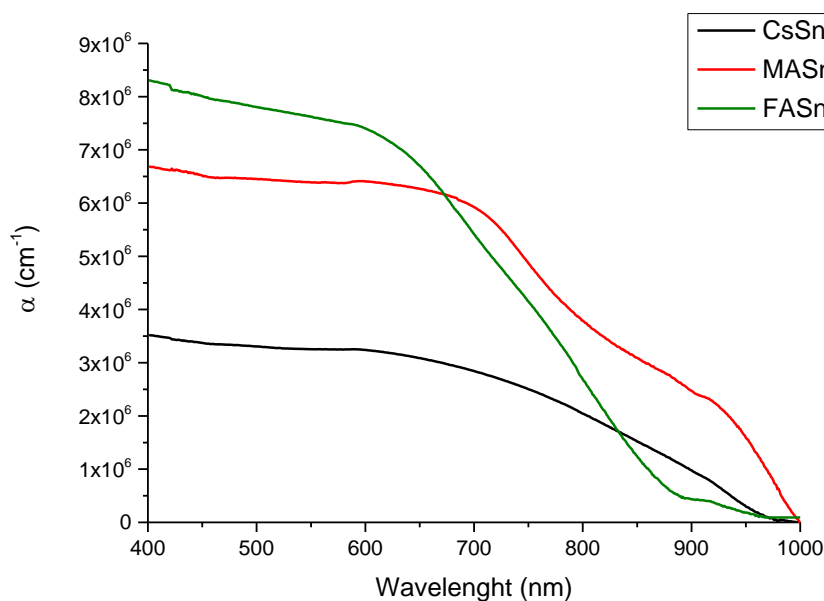


Figure 16: UV/Vis absorption spectra of single cation Sn – perovskites

The absorption of the prepared perovskites (Fig. 16) shows high absorption over a wide wavelength range, which also matches well with the dark grey/black colour of the perovskite layers. FASnI_3 has a good visible onset at 880 nm and the highest absorption coefficient compared to the other ones at lower wavelengths. MASnI_3 has an early onset at 1000 nm and a slight shoulder behaviour from 720 nm to 940 nm. The absorption curves for FA- and MA-based tin perovskites match well with literature^{98,100,107}. The absorption spectrum of CsSnI_3

was not in good accordance with literature due to a shift of the onset to higher wavelengths as reported¹⁰⁸.

In addition, band gap energies (E_g) of the materials were calculated using Tauc-Plot. The absorption coefficient (α) was calculated according to formula 3.

$$\alpha = 2.3026 * \frac{A}{t} \quad (3)$$

α = absorption coefficient [cm^{-1}]

A = absorbance []

t = layer thickness [cm]

The layer thickness values were obtained from five experimental values and the mean value was taken into account for calculations. (Tab. 11)

Table 11: Layer thickness values of single cation tin perovskites, mean values and standard deviation

Sample	Thickness [nm]
CsSnI₃	517 ± 140
MASnI₃	243 ± 4
FASnI₃	248 ± 16

Since the materials have a direct allowed electron transition E_g was graphically identified by plotting $(\alpha h\nu)^2$ against the photon energy ($h\nu$) and extrapolating the linear part of the generated curves to intersect the x-axis. (Fig. 17) The intersection point is equivalent to the band gap of the material.

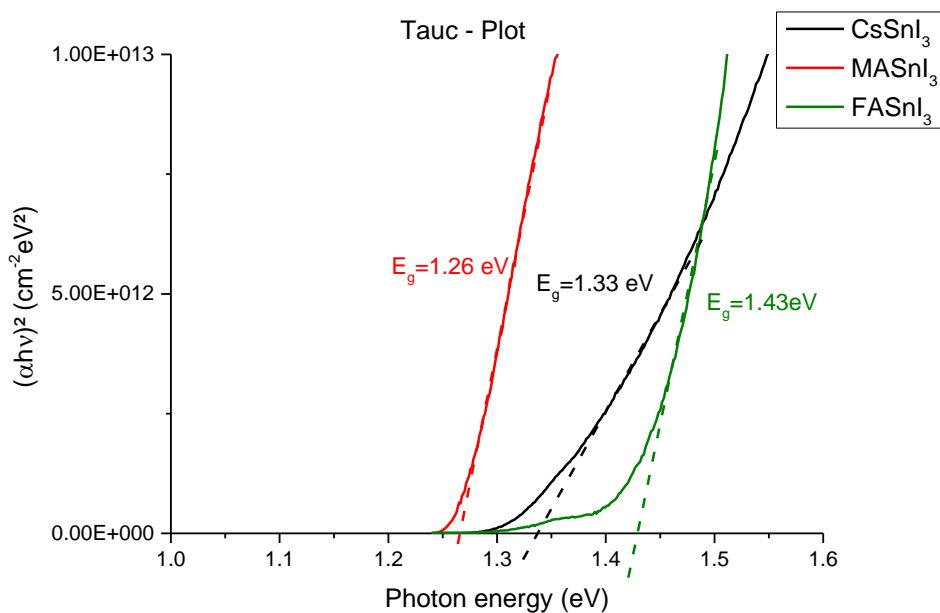


Figure 17: Tauc-plot of single cation Sn-perovskites

Band gap values of all investigated single cation tin perovskites match very well with literature.^{95,98,109} (Tab. 12) It is shown that MASnI₃ is a low band gap material, whereas the band gap widens when exchanging the cation to FASnI₃.

Table 12: Band gap values for tin perovskites, experimental data and literature values^{95,98,109}

Perovskite	Band gap (literature) [eV]	Band gap (experimental) [eV]
CsSnI ₃	1.30	1.33
MASnI ₃	~1.25 – 1.3	1.26
FASnI ₃	~1.4	1.43

4.1.2 XRD analysis

XRD-measurement of the single crystal perovskites MASnI₃ and FASnI₃ (Fig. 18 and 19) was done to investigate their crystallographic structure. Since absorption did not match exactly in the case of CsSnI₃ and time was limited, XRD data of CsSnI₃ was not obtained.

XRD-diffractograms of the formed perovskites were in good accordance with literature.^{90,105} The (h k l) indices of lattice planes were associated with the peaks, where information was available.

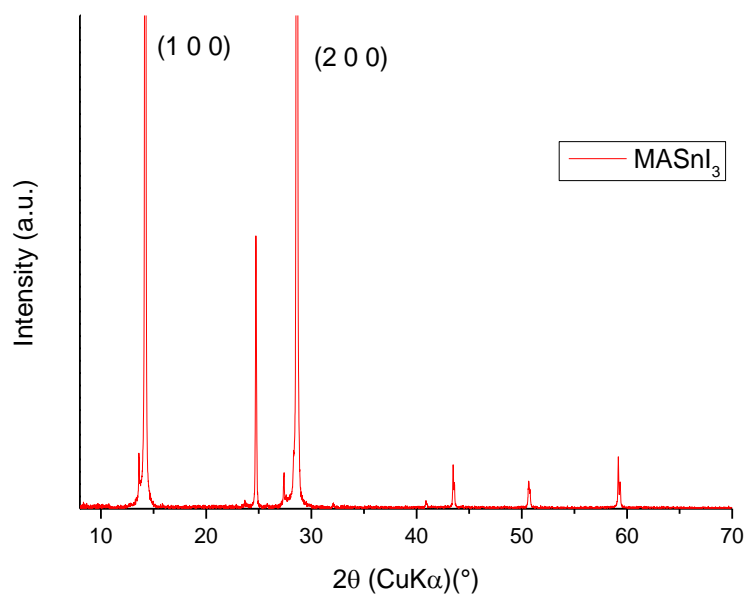


Figure 18. XRD diffractogram of MASnI₃

In case of MASnI₃ the two distinctive main peaks at 14° and 28° 2θ are characteristic for the material and refer to the (1 0 0) and (2 0 0) lattice plains respectively. Further, the diffractogram indicate a 3D crystal structure as expected.

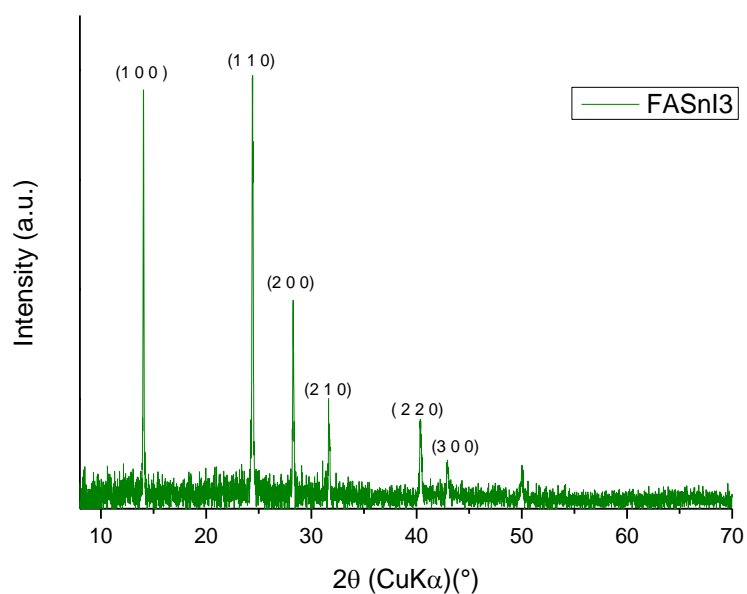


Figure 19: XRD diffractogram of FASnI₃

For FASnI₃ the diffraction pattern also indicates a 3D structure and has two main peaks at 14° and 28° 2θ, same as MASnI₃. These refer to the (1 0 0) and (2 0 0) lattice plains respectively

and are characteristic for Sn-perovskites. Also a peak at $24^\circ 2\theta$, referring to the (1 1 0) is dominant.

4.1.3 Solar cell performance

To investigate the material for use in solar cell applications, relevant solar cell characteristics were measured and compared to each other and literature values. Solar cell performance was derived from IV-measurement for CsSnI_3 , MASnI_3 , FASnI_3 , with the device structure ITO/PEDOT:PSS/perovskite/ $\text{PC}_{60}\text{BM}/\text{Al}$.

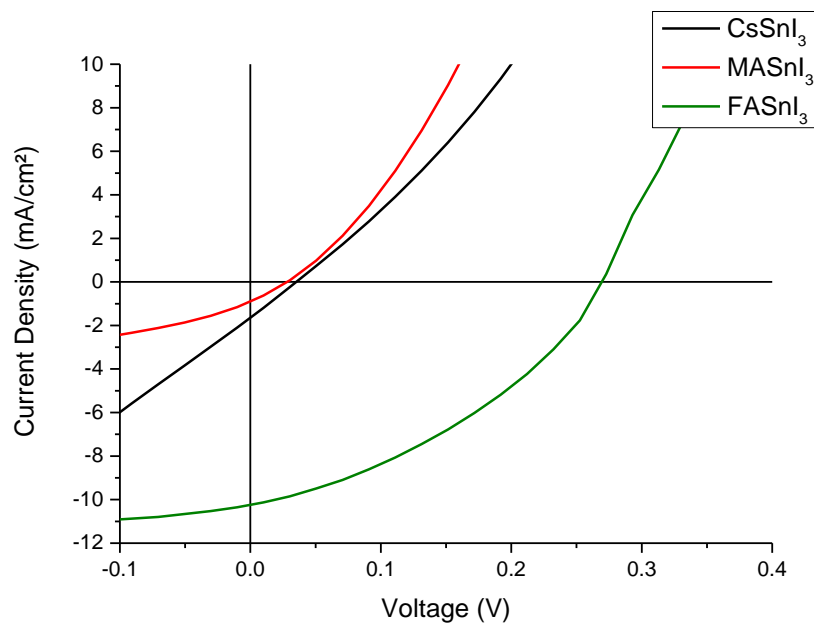


Figure 20: IV-curves of single cation Sn-perovskites

Although measurements were done from a voltage -1 V to +1 V, only region of -0.1 V to +0.4 V is illustrated to get a more detailed view on the relevant solar cell parameters (Fig. 20, Tab. 13).

Table 13: Mean solar cell parameters of single cation tin perovskites. Mean values were obtained from five best cells. Best cell values were chosen in with regards to highest efficiency.

Sample	PCE [%]	V _{oc} [mV]	J _{sc} [mA/cm ²]	FF [%]
CsSnI ₃	0.004 ± 0.003	15.1 ± 8.7	1.6 ± 0.3	12.6 ± 5.9
Best	0.012	30.3	2.1	18.9
MASnI ₃	0.006 ± 0.001	30.3 ± 0.01	1.1 ± 0.1	17.2 ± 2.2
Best	0.007	30.3	1.2	19.9
FASnI ₃	0.76 ± 0.17	256.6 ± 15.1	9.0 ± 1.0	32.5 ± 2.3
Best	1.03	272.8	10.3	36.6

It was not possible in this setup to produce functioning CsSnI₃ solar cells with even average efficiency. MASnI₃ has a more distinct diode characteristic, but still has low performance values. Further FASnI₃ has the highest efficiency and also the best solar cell performance, regarding experimental data, but is also below literature values for all characteristics. Since to the best of my knowledge this were the first experiments of producing CsSnI₃ solar cells in this specific setup, one can assume that this device architecture is not suitable for a pure inorganic tin perovskite solar cell. Literature showed that a different HTL is more suitable for CsSnI₃.⁹² Further optimization of relevant parameter or testing a variety of different HTL or ETL combinations could possibly lead to better functioning solar cells. However, this was not deeper investigated in this thesis. Moreover, the characteristic values for MASnI₃ did not match the best reported values by far, although the fabrication method was very similar to literature.¹⁰² (Tab.13) The reasons for this could be manifold. One possible explanation for this might be the use of impure SnI₂, which, as mentioned before, has a drastic influence on solar cell efficiency. Furthermore, layer thickness of almost all involved layers (HTL, perovskite, ETL) varies from literature¹⁰² and has also a big impact on solar cell values like V_{oc} and J_{sc}. The same can be said for FASnI₃, since device fabrication, although not exactly the same, is similar to literature¹⁰⁰. Low values for J_{sc} could also be indicating the bad quality of SnI₂ used. In addition, it is not clear, to what account other problems like pinholes, layer morphology, miss aligned energy levels or short circuits, are responsible for the low efficiencies.

Table 14: Best Sn-based perovskite solar cell performance published in literature

Perovskite	PCE [%]	V _{oc} [mV]	J _{sc} [mA/cm ²]	FF [%]
MASnI ₃ ⁹⁸	6.4	880	16.8	42
CsSnI ₃ ⁹⁵	2.0	240	22.7	37
FASnI ₃ ⁹⁹	5.3	380	23.1	60

4.2 DOUBLE CATION SN-PEROVSKITES

It was also subject of this thesis to reproduce the work of Liao et al.¹⁰⁵ and further test the influence of PEAI as additional cation to various tin halide perovskites. These results however were so manifold that they will be discussed separately in chapter 4.3.

Based on the work of Zhao et al.¹⁰¹ a double cation perovskite, based on a mix of MA⁺ and FA⁺ cations, was prepared and characterised with regard to its optical and crystallographic properties, as well as on its solar cell performance. Since the reported best molar ratio of MA⁺ to FA⁺ ions was 0.75/0.25, the focus in this work was laid solely on this cation composition.

4.2.1 Optical characterisation

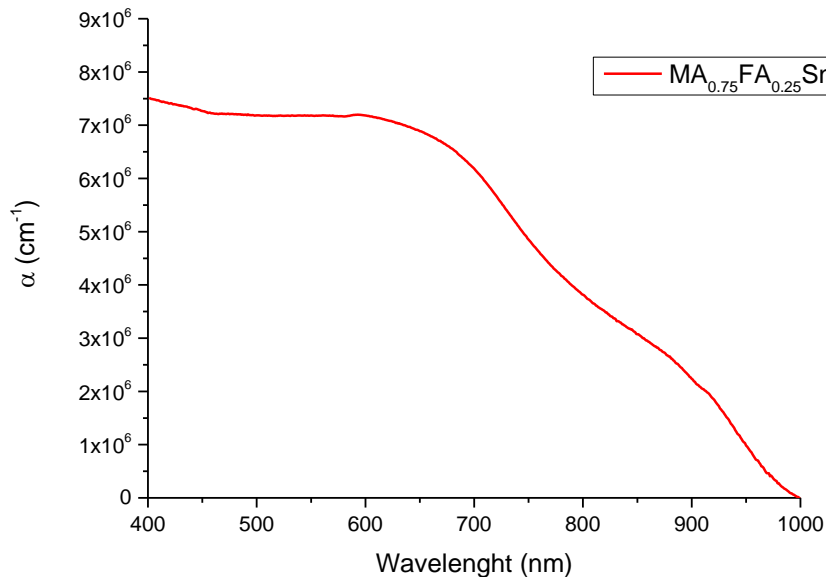


Figure 21: UV/Vis absorption of MA_{0.75}FA_{0.25}SnI₃ perovskite

Absorption of the prepared tin perovskite matches not exactly the reported spectrum in literature,¹⁰¹ although some similarity can be seen. (Fig. 21) The absorption plateau start at a wavelength of 600 nm and the slight shoulder in the range of 850 nm to 700 nm match with

the references, but the onset at 1000 nm differs, since the reported onset is not shown below 1100 nm.

Tauc-plot of the perovskite (Fig. 22) was calculated with the same method as described in chapter 4.1.1. The layer thickness taken into account was 248 ± 5 nm.

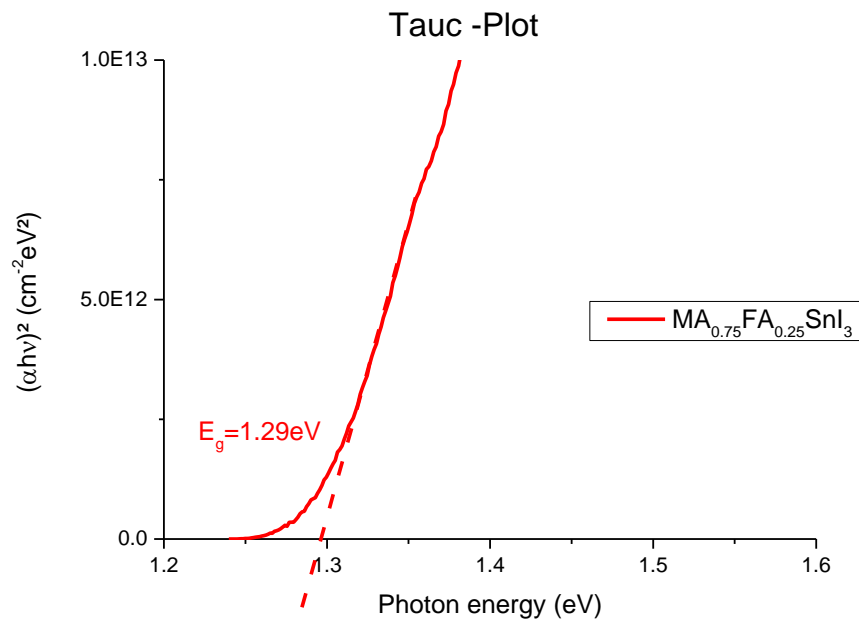


Figure 22: Tauc-plot of MA_{0.75}FA_{0.25}SnI₃ perovskite

The graphically determined band gap value of 1.29 eV matches very well with the published band gap energy of 1.28 eV from literature.¹⁰¹ Low band gap values derived from high amount of MA⁺ and low amount of high band gap FA⁺, thus resulting in a slight increase in band gap, compared to pure MASnI₃. (Fig. 17)

4.2.2 XRD analysis

To get a better understanding of the material, XRD-measurements were done to obtain crystallographic data. (Fig. 23)

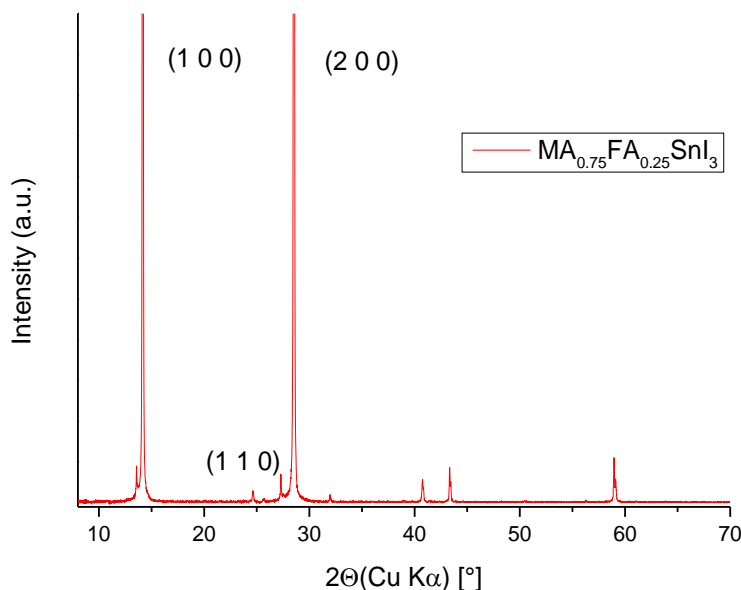


Figure 23: XRD-diffractograms of MA_{0.75}FA_{0.25}SnI₃ perovskite

The given XRD data matches well with the data published in literature.¹⁰¹ The three main diffraction peaks at 14°, 24° and 28° 2θ, refer to the (1 0 0), (1 1 0) and (2 0 0) lattice planes respectively and are characteristic for Sn-perovskites. They can also be observed in the XRD diffractograms of MASnI₃ and FASnI₃. Compared to the diffractogram of FASnI₃ (Fig. 19) the peaks at 32° and 41° 2θ are also present, but with lower intensity, due to a lower amount of FA⁺ in the crystal structure. This indicates that MA⁺ and FA⁺ are equally distributed in the crystal lattice, forming only a MA_{0.75}FA_{0.25}SnI₃ perovskite, instead of phases composed of MASnI₃ and FASnI₃.

4.2.3 Solar cell performance

To investigate the double cation perovskite in regards of its use in solar cell applications, IV-measurement was done and obtained data was compared to literature values.

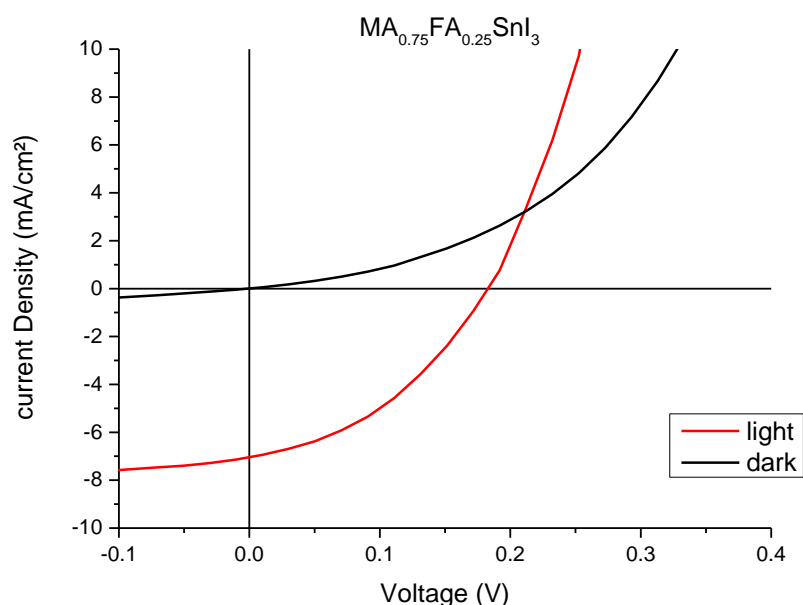


Figure 24: IV – curves of $MA_{0.75}FA_{0.25}SnI_3$ perovskite, measurements in the dark and under illumination

Solar cells made from the mentioned double cation perovskite show a working diode behaviour (Fig. 24), but with low values regarding all characteristics. (Tab. 15) The resulting data is far below the values expected from literature.¹⁰¹ Reasons for this can be the same as in the single cation tin perovskites, mentioned in chapter 4.1.2., impurities of SnI_2 , slight differences in architecture and variety in layer thickness.

Table 15: Solar cell characteristics of $MA_{0.75}FA_{0.25}SnI_3$ perovskite. Mean values were obtained from five best cells. Best cell values were chosen in with regards to highest efficiency

	PCE [%]	V_{oc} [mV]	J_{sc} [mA/cm ²]	FF [%]
Mean	0.43 ± 0.07	171.7 ± 14.3	6.3 ± 0.7	39.2 ± 1.8
Best	0.51	191.9	7.1	37.1
Literature	8.12	610	21.2	62.7

4.3 INTRODUCTION OF PEA⁺ CATION

As mentioned above, the influence of PEA⁺ cation incorporated in an organic/inorganic tin halide perovskite was deeper investigated. All mentioned single cation perovskites ($CsSnI_3$, $MASnI_3$ and $FASnI_3$) were produced with a 20 mol% substitution of PEA⁺. The amount was chosen based on the work of Liao et al.¹⁰⁵, due to the fact that 20 mol% substitution rendered

the highest efficiency values. The focus point was on the change in optical properties, crystallographic structure and solar cell characteristics.

4.3.1 Changes in optical properties

With the introduction of PEA^+ as additional cation in the perovskite structure, one can see some significant changes in the optical properties.

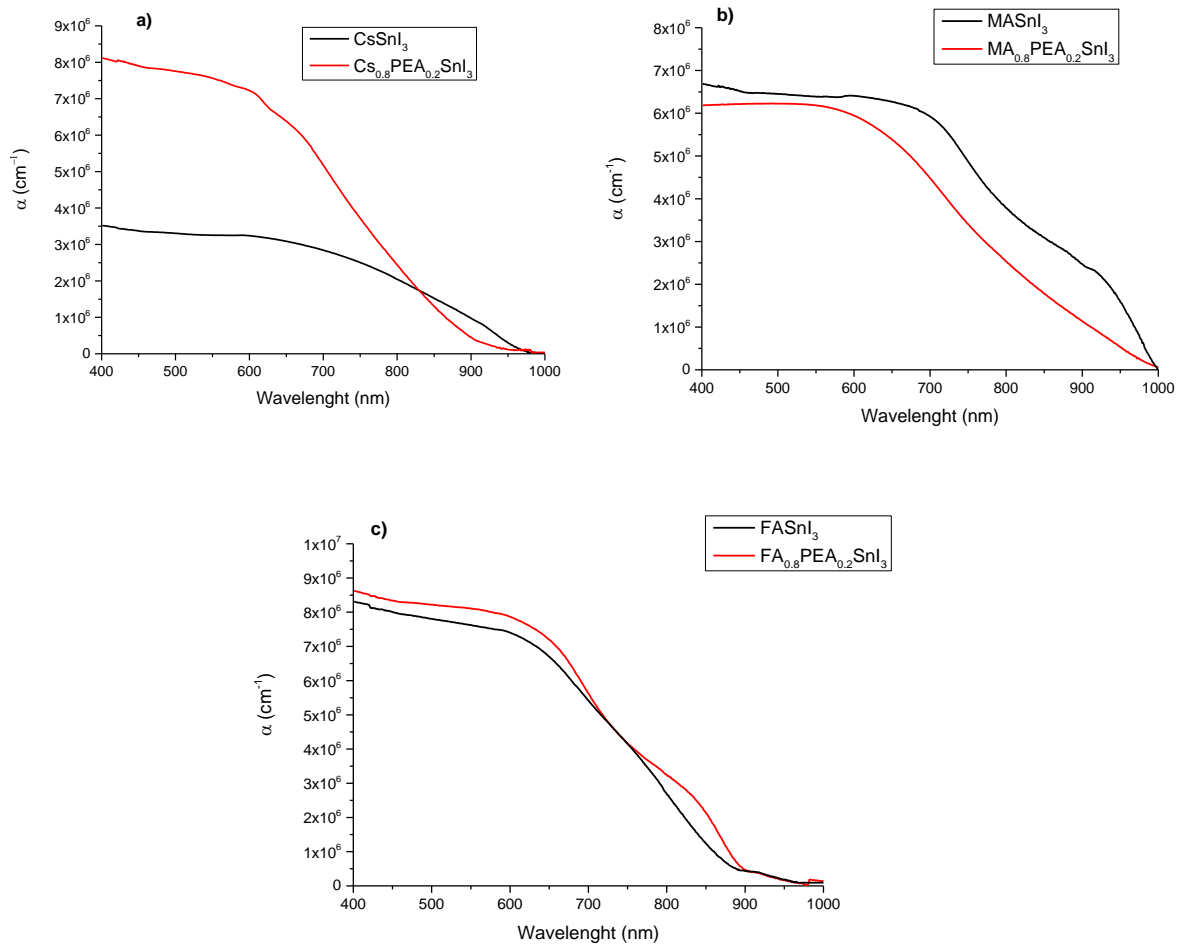


Figure 25: Absorption spectra of a) CsSnI_3 b) MASnI_3 and c) FASnI_3 and their corresponding absorption with 20 mol% PEA^+ substitution

In the case of CsSnI_3 (Fig. 25; a), which is a pure inorganic perovskite, the addition of the organic PEA^+ cation shifts the absorption onset to lower wavelengths. In addition, absorption in the area of low energetic wavelengths decreases, whereas absorption increases in the range below 820 nm. Concerning MASnI_3 (Fig. 25; b) absorption decreases, due to a shift to higher band gaps. In addition, curve behaviour changes from a shoulder formed increase to a straight rise in absorption. On the matter of FASnI_3 , (Fig. 25; c) a slight shift of the onset line to higher wavelength is observed, as well as onset shape changes from a straight increase in absorption

to a shoulder formation between 850 nm and 700 nm. This is in good accordance with the provided spectra from literature¹⁰⁵. Overall, the absorption has a slight increase over the whole spectrum.

Moreover, the change of the optical band gap energy was calculated from absorptions utilising the same calculation pathway as described in chapter 4.1.1. with layer thickness values taken from Tab. 16.

Table 16: perovskite layer thickness of $A_{0.8}PEA_{0.2}SnI_3$ ($A = Cs, MA, FA$)

Sample	thickness [nm]
$Cs_{0.8}PEA_{0.2}SnI_3$	267 ± 46
$MA_{0.8}PEA_{0.2}SnI_3$	292 ± 13
$FA_{0.8}PEA_{0.2}SnI_3$	236 ± 15

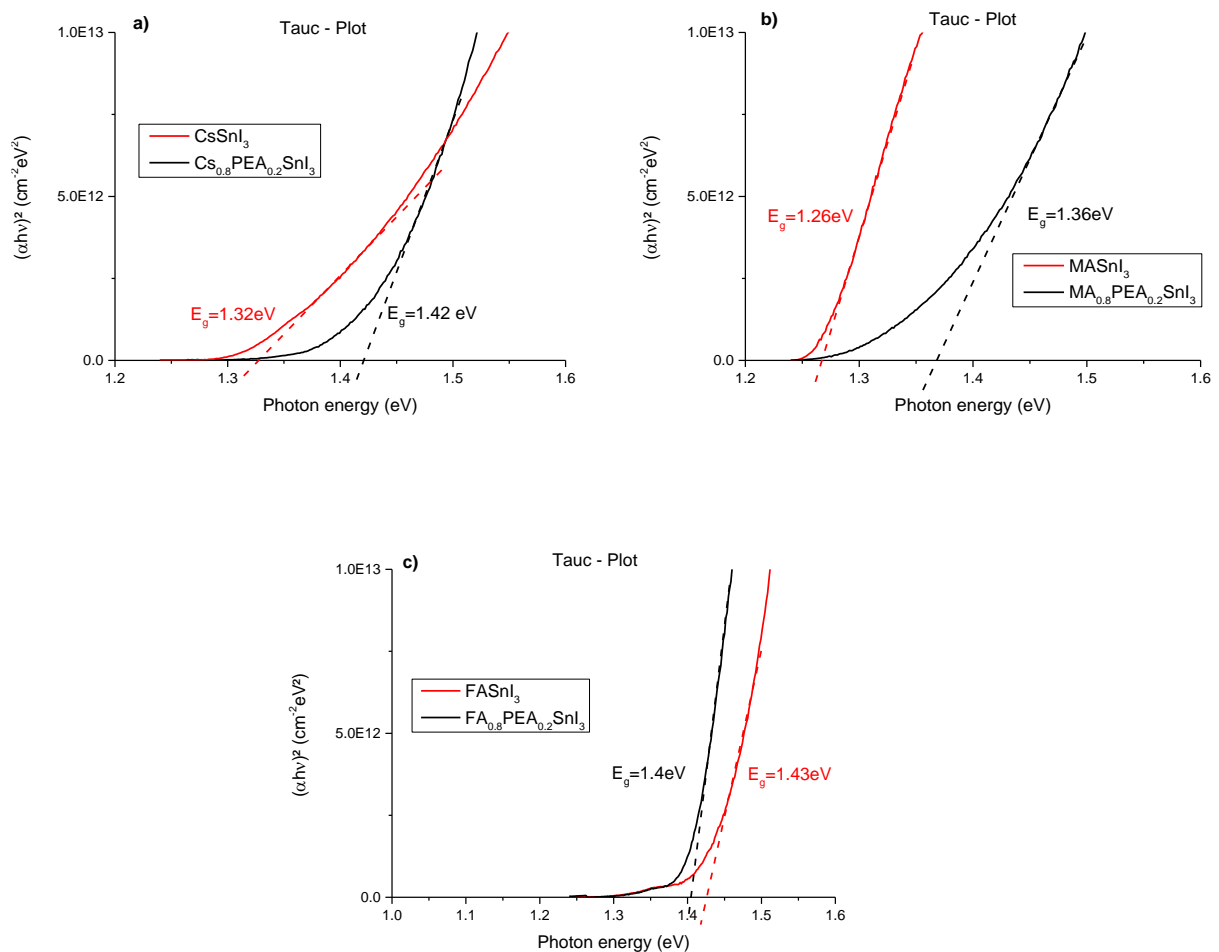


Figure 26: Band gap values of a) $CsSnI_3$ b) $MASnI_3$ and c) $FASnI_3$ and their corresponding mixed cation equivalent with 20 mol% PEA^+ substitution

The band gap values for Cs- and MA-based tin perovskites (Fig. 26; a, b) increase, with the substitution of PEA⁺, by 0.1 eV. This matches well with the absorption data (Fig. 25; a, b) since a lower onset value in absorption contributes to a higher optical band gap value. In case of FASnI₃ (Fig. 26, c) the band gap lowers by 0.03 eV, which is also in accordance with the detected absorption.

4.3.2 XRD analysis

To observe the change in crystallographic properties and to confirm the formation of a 2D structured perovskite, XRD analysis of FA_{0.8}PEA_{0.2}SnI₃ and MA_{0.8}PEA_{0.2}SnI₃ was done and compared to the data of the single cation perovskites.

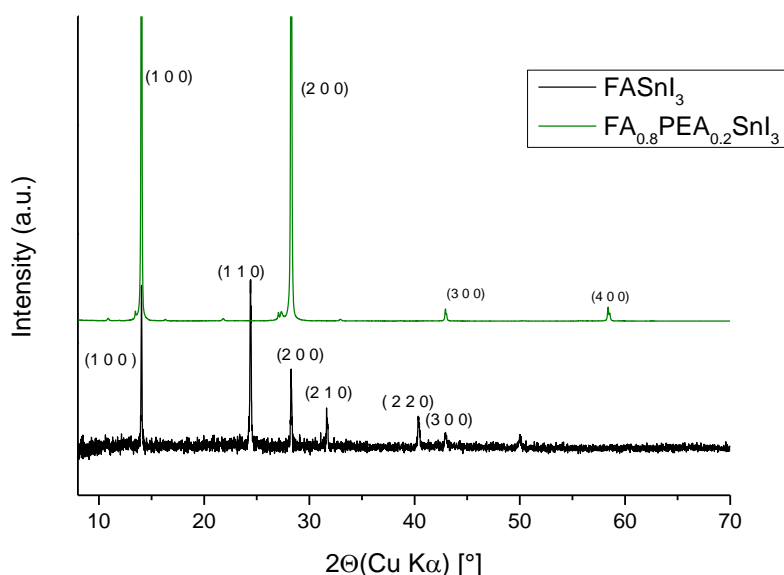


Figure 27: XRD diffractograms of FA_{0.8}PEA_{0.2}SnI₃ perovskite compared to FASnI₃

The data gathered from XRD (Fig. 27) matches well with the information on crystal structure from literature.^{105,106} Crystalline phases of FASnI₃ are separated by organic interlayers composed of PEA⁺ aromatic groups, arranged to each other. The indices were taken from literature where information was available. The vanishing of the peaks at 24°, 32°, 41° and 50° 2θ indicates, that with the introduction of PEA⁺ a system of mixed 3D and 2D perovskite structure is formed.¹⁰⁵ Also the four distinct peaks at 14°, 28°, 43° and 58° 2θ, referring to the (1 0 0), (2 0 0), (3 0 0) and (4 0 0) lattice planes respectively, indicate a layered structure.

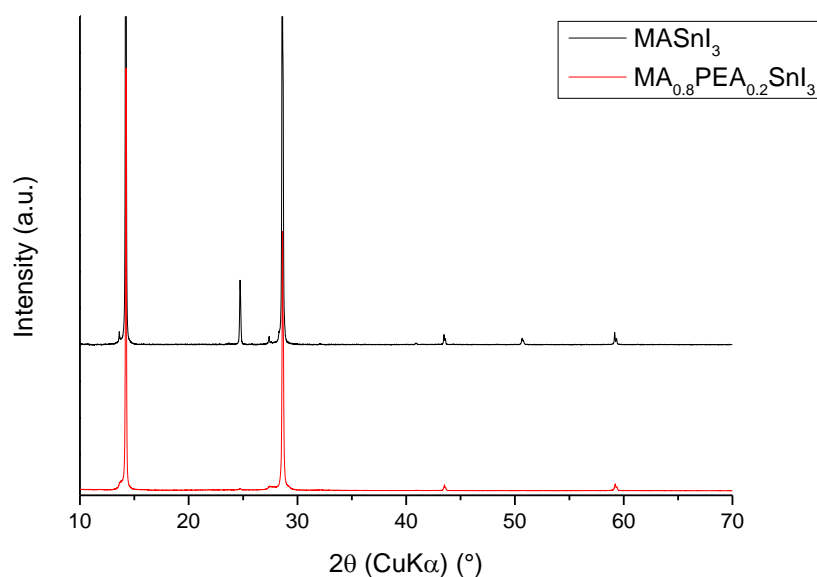


Figure 28: XRD diffractograms of $MA_{0.8}PEA_{0.2}SnI_3$ perovskite compared to $MASnI_3$

The main peaks in this data (Fig. 28) show slight changes, in the form of vanishing peaks. Peaks at angles of 24° and 52° 2θ vanish on addition of PEA^+ . This indicates, similar to $FASnI_3$, the formation of a 2D structure in the perovskite material. The layered structure is further confirmed by the four distinct peaks at 14° , 28° , 44° and 59° 2θ , referring to the (1 0 0), (2 0 0), (3 0 0) and (4 0 0) lattice planes respectively.

4.3.3 Solar cell performance

To confirm the correlation between the changes in optical and crystallographic properties, IV-measurements were done, and the change in solar cell performance was discussed.

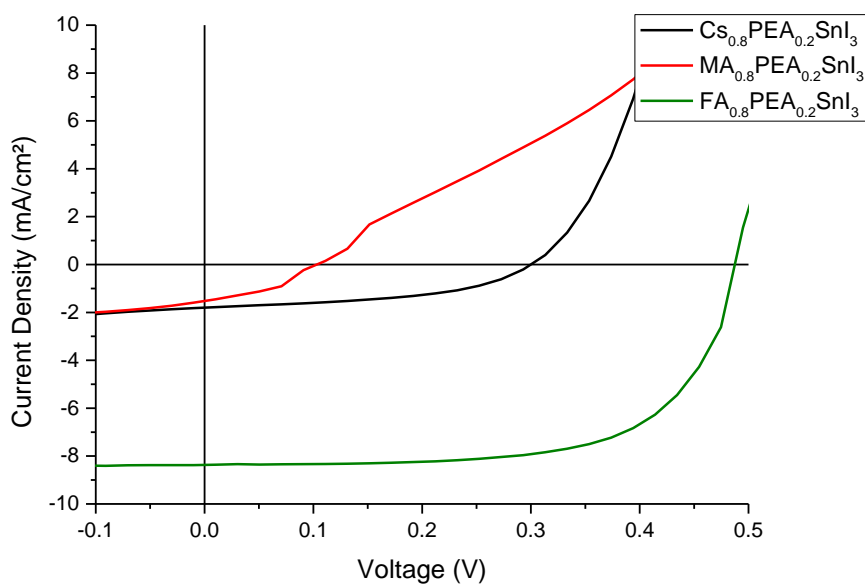


Figure 29: IV-curves of $A_{0.8}PEA_{0.2}SnI_3$ ($A = Cs, MA, FA$) mixed cation perovskites

The IV-data of different perovskites mixed with PEA^+ (Fig. 29) shows an increase in all solar cell characteristics, for all investigated materials. (Tab. 17). Overall the values for V_{oc} rises the most. Values for J_{sc} suffers a slight decrease, indicating that the amount of PEA^+ changes the quantity of charge carriers in the systems. This concludes that substituting a small amount of an A-side ion with an optical inactive species might reduce the number of extractable charges. The change from $MASnI_3$ to $MA_{0.8}PEA_{0.2}SnI_3$ increases mainly the V_{oc} value, which could be expected since the band gap energy increases as well. However, PCE values are still far from competitive with similar device architectures.¹⁰⁵ In the case of $Cs_{0.8}PEA_{0.2}SnI_3$, contrary to $CsSnI_3$, it was possible to fabricate solar cells with a diode curve behaviour and, similar to the MA – based perovskite, to enhance the open circuit voltage. Concerning $FA_{0.8}PEA_{0.2}SnI_3$, the PCE increases drastically from 0.76 % to 2.06 % due to an enormous rise in V_{oc} and FF. Nonetheless the reported 6.22 % PCE achieved with this material¹⁰⁵ was, with only a third of literature efficiency values, not reached. Reasons for the lack of efficiency might be similar to that in single cation case. The low value for J_{sc} could originate from impurities in the chemicals, since it is a common problem in tin halide perovskites to loose J_{sc} to contaminations already present in starting chemicals or forming during device fabrication. Another problem could be the comparability from this experiment to the reference taken from literature due to the different HTL, namely PEDOT:PSS instead of NiO_x .

Table 17: solar cell characteristics of $A_{0.8}PEA_{0.2}SnI_3$ ($A = Cs, MA, FA$) mixed cation perovskites and best cell values. Mean values were obtained from five best cells. Best cell values were chosen in with regards to highest efficiency

Sample	PCE [%]	V_{oc} [mV]	J_{sc} [mA/cm ²]	FF [%]
Cs_{0.8}PEA_{0.2}SnI₃	0.12 ± 0.06	275.3 ± 18.7	0.95 ± 0.4	43.9 ± 5.4
Best	0.25	293.0	1.8	47.9
MA_{0.8}PEA_{0.2}SnI₃	0.05 ± 0.02	184.3 ± 77.7	1.06 ± 0.5	27.5 ± 5.8
Best	0.10	252.5	2.1	19.9
FA_{0.8}PEA_{0.2}SnI₃	2.06 ± 0.32	488.2 ± 9.5	7.1 ± 0.8	60.7 ± 3.8
Best	2.69	495.0	8.4	65.2

4.4 TRIPLE CATION SN – PEROVSKITE

As another task to investigate the influence of different cations and cation composition in tin halide perovskites, a combination of perovskites that have shown good long term stability, like the PEA^+ enhanced $FASnI_3$ ¹⁰⁵, and high efficiency, like $MA_{0.75}FA_{0.25}SnI_3$ ¹⁰¹, was tested with regard to photovoltaic efficiency and also optical and crystallographic properties. This triple cation material consisting of a tin halide perovskite with MA^+ , FA^+ and PEA^+ as cations was compared to the previously mentioned double cation $MA_{0.75}FA_{0.25}SnI_3$ perovskite, more promising in all preceding noted categories. (Chapter. 4.2.) Since the best working composition of double cation perovskite was $MA_{0.75}FA_{0.25}SnI_3$ and literature shows a rise in efficiency with higher MA^+ content it was decided to leave the content of MA^+ at 75 mol% and add PEA^+ in 10 mol% and 20 mol% amount, decreasing the amount of FA^+ accordingly, to maintain stoichiometry. Since with higher amounts of FA^+ solar cell characteristics (Chapter. 4.4.3) are much higher, optical and crystallographic characterisation was only done for $MA_{0.75}FA_{0.15}PEA_{0.1}SnI_3$ and compared to the non- PEA^+ equivalent.

4.4.1 Optical characterisation

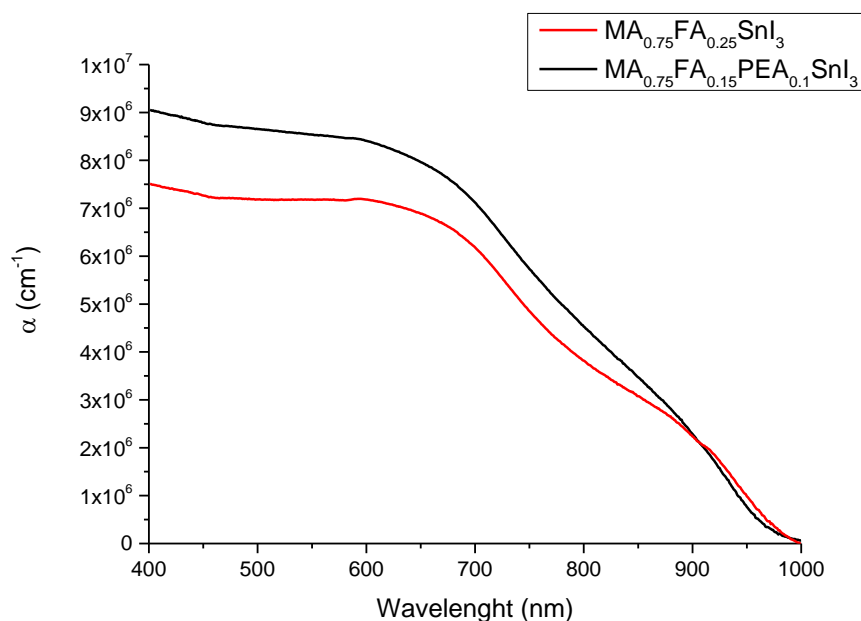


Figure 30: UV/Vis absorption of triple cation $\text{MA}_{0.75}\text{FA}_{0.15}\text{PEA}_{0.1}\text{SnI}_3$ compared to double cation $\text{MA}_{0.75}\text{FA}_{0.25}\text{SnI}_3$

Optical absorption (Fig. 29) of the perovskite material increases when going from a double cation to a triple cation perovskite. With the introduction of PEA^+ , a similar effect, like in the case of introducing PEA^+ in MASnI_3 perovskite, can be observed. Absorption increases in the range below 900 nm compared to the double cation without PEA^+ . The onset is almost unchanged and is positioned at a relatively high wavelength of 1000 nm, due to the high amount of MA^+ present.

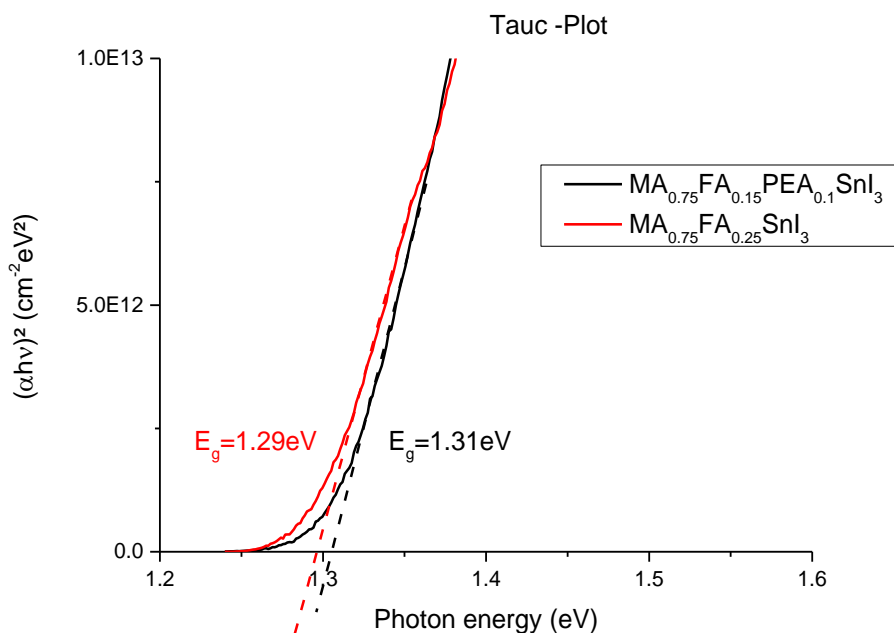


Figure 31: Band gap energies of triple cation $MA_{0.75}FA_{0.15}PEA_{0.1}SnI_3$ compared to double cation $MA_{0.75}FA_{0.25}SnI_3$

To obtain optical band gap values a Tauc-plot was done utilising the same mathematic procedure as described in chapter. 4.1.1. The mean layer thickness value for $MA_{0.75}FA_{0.15}PEA_{0.1}SnI_3$ was 232 ± 14 nm.

The Tauc-Plot of triple cation perovskite $MA_{0.75}FA_{0.15}PEA_{0.1}SnI_3$ (Fig. 31) shows a slight increase in the optical band gap energy. This is well in accordance with the slight shift in absorption onset and matches the expectations, which can be predicted from the increase in optical band gap in $MASnI_3$, when substituting a small amount of MA^+ with PEA^+ . (Fig. 26, b)

4.4.2 XRD analysis

XRD-measurement was done to confirm the change from a 3D to a 2D structure, upon addition of PEA^+ . The obtained data was compared to the XRD-diffractogram of the double cation perovskite $MA_{0.75}FA_{0.25}SnI_3$.

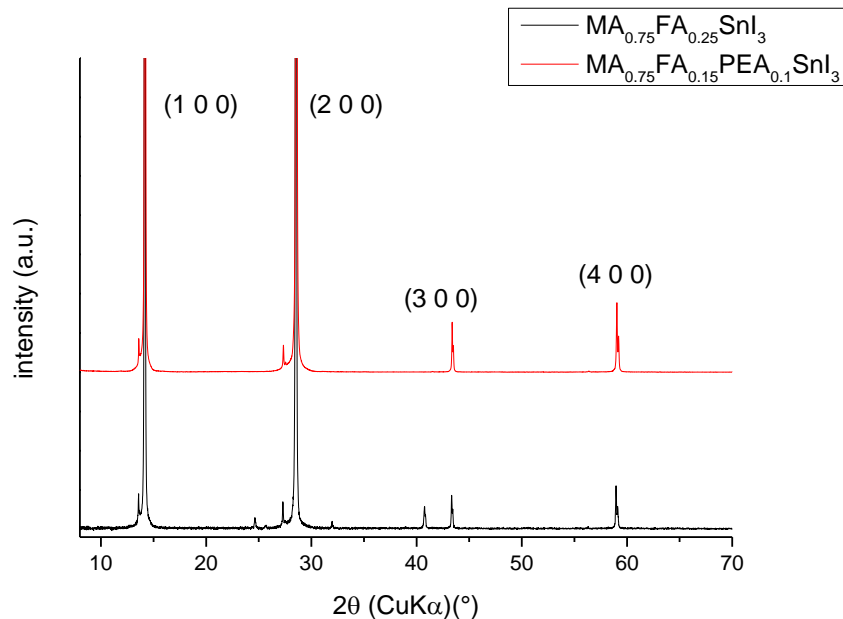


Figure 32: XRD diffractograms of triple cation $MA_{0.75}FA_{0.15}PEA_{0.1}SnI_3$ compared to double cation $MA_{0.75}FA_{0.25}SnI_3$

The given XRD data (Fig. 32) confirms the formation of a 2D perovskite structure in the triple cation perovskite. The main peaks at 14° , 28° , 43° and 58° 2θ are well in accordance with the expected peaks, derived from literature, indicating a strong orientation in the structure.^{101,105} The peaks at 24° , 32° and 41° 2θ indicating a crystalline cubic $FASnI_3$ phase vanishes with the introduction of PEA^+ , which matches well with the formation of an organic layer between crystalline phases. This phenomenon is also observed in the XRD diffractogram of $FASnI_3$, at the incorporation of PEA^+ to form $FA_{0.8}PEA_{0.2}SnI_3$.¹⁰⁵

4.4.3 Solar cell performance

IV-measurements of triple cation $MA_{0.75}FA_{0.15}PEA_{0.1}SnI_3$ and $MA_{0.75}FA_{0.05}PEA_{0.2}SnI_3$ show the increase in solar cell performance compared to $MA_{0.75}FA_{0.25}SnI_3$. In addition, the influence of a different composition of the cations on solar cell performance was investigated and the experimental data was compared.

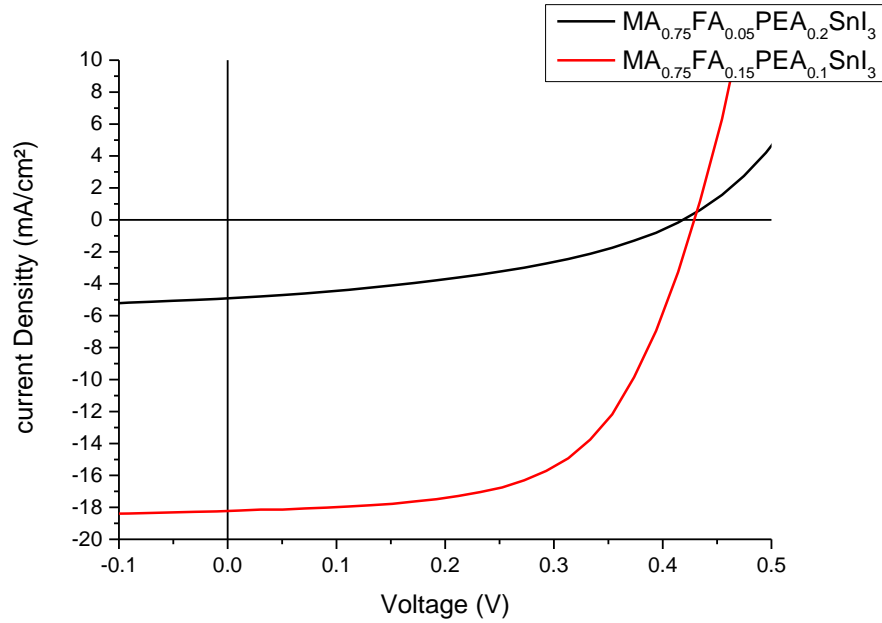


Figure 33: IV curves of $MA_{0.75}FA_{0.15}PEA_{0.1}SnI_3$ and $MA_{0.75}FA_{0.05}PEA_{0.2}SnI_3$

The compared IV-characteristic of the produced triple cation perovskites (Fig. 33) shows a big increase in all values, when the amount of PEA^+ is reduced to 10 mol% and FA^+ is set to 15 mol%. Cation composition in the case of $MA_{0.75}FA_{0.05}PEA_{0.2}SnI_3$ renders lower values in PCE, J_{sc} and FF and the curve resembles more that of $MA_{0.8}PEA_{0.2}SnI_3$. The solar cell performance of the manufactured triple cation perovskite $MA_{0.75}FA_{0.15}PEA_{0.1}SnI_3$ was over all the best of all experiments done during this thesis. (Tab. 18).

Table 18: solar cell characteristics of triple cation perovskites. Mean values were obtained from five best cells. Best cell values were chosen in with regards to highest efficiency

Sample	PCE [%]	Voc [mV]	Jsc [mA/cm ²]	FF [%]
$MA_{0.75}FA_{0.05}PEA_{0.2}SnI_3$	0.67 ± 0.07	414.2 ± 12.8	4.6 ± 0.3	36.1 ± 2.7
Best	0.81	414.2	5.0	39.8
$MA_{0.75}FA_{0.15}PEA_{0.1}SnI_3$	4.39 ± 0.2	430.3 ± 8.1	17.6 ± 0.7	58.8 ± 2.6
Best	4.60	434.3	18.2	59.0

4.4.4 EQE measurement

Furthermore external quantum efficiency (EQE) measurements were done and compared to the UV/Vis absorption spectra.

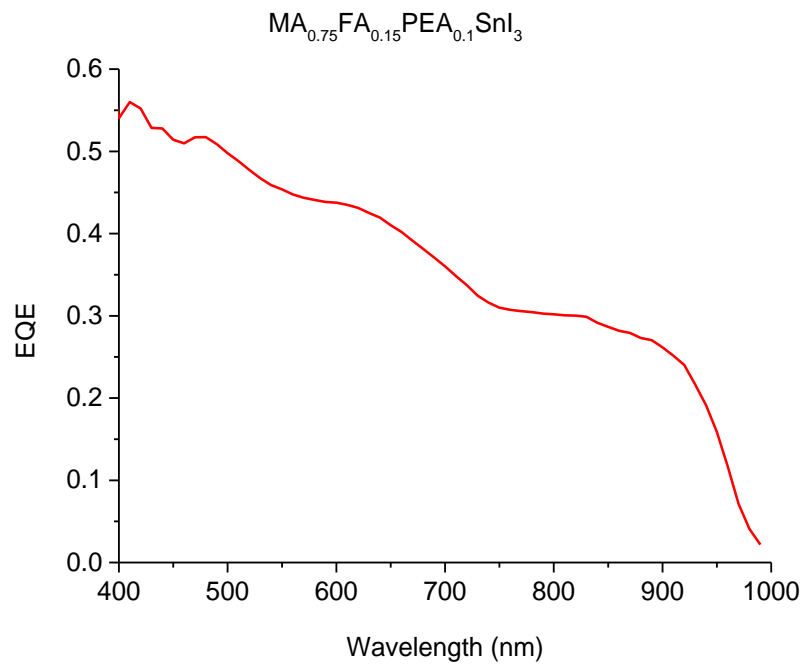


Figure 34: EQE measurement results of $MA_{0.75}FA_{0.15}PEA_{0.1}SnI_3$

The given EQE data (Fig. 34) indicates some major differences from the measured UV/Vis absorption. (Fig. 30) Although a small step in UV/Vis absorption is visible around 920 nm, it is not comparable to the plateau of the EQE measurement, reaching from 920 nm to 740 nm. Furthermore, the increase in absorption in a wavelength range below 650 nm did not match the plateau in the absorption spectrum.

4.4.5 Hysteresis behaviour

To see the influence of hysteresis, the difference in IV-characteristics running the device in backwards bias compared to forward bias, the best performing solar cell device was measured in both voltage directions, forwards, from -1 V to +1 V, and backwards, from +1 V to -1 V. (Fig. 35)

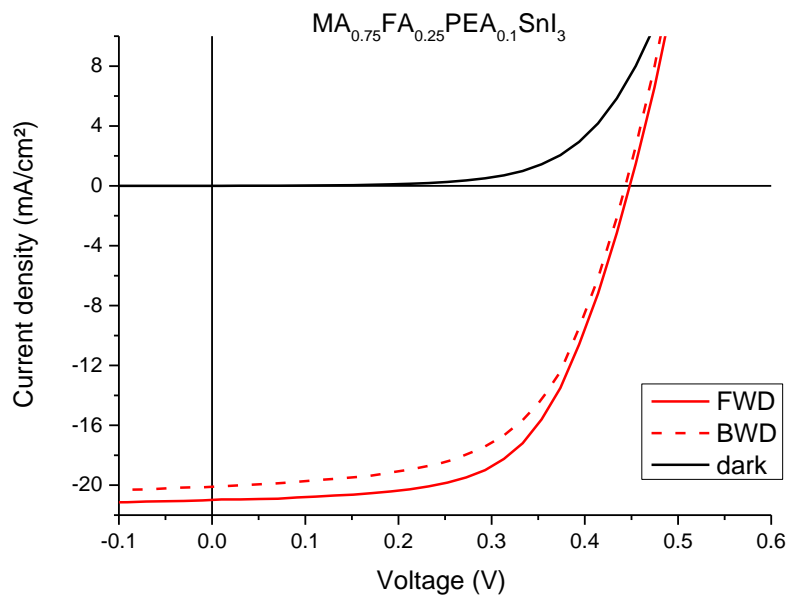


Figure 35: Hysteresis behaviour of triple cation $MA_{0.75}FA_{0.15}PEA_{0.1}SnI_3$

A slight difference in V_{oc} and J_{sc} can be observed from measuring with backward bias. However, since the change in all characteristic value is below 10%, (Tab. 19) hysteresis behaviour in the case of $MA_{0.75}FA_{0.15}PEA_{0.1}SnI_3$ is rather low.

Table 19: solar cell performance triple cation $MA_{0.75}FA_{0.15}PEA_{0.1}SnI_3$ in forward and backward bias. Mean values of best five cells. Best cell values was taken regarding best efficiency

	PCE [%]	Voc [mV]	Jsc [mA/cm ²]	FF [%]
forward	5.32 ± 0.35	454.6 ± 0.1	20.5 ± 0.6	58.2 ± 2.4
Best	5.63	454.6	21.3	59.3
backward	4.95 ± 0.25	442.4 ± 9.9	19.4 ± 0.7	58.9 ± 2.2
Best	5.16	434.4	20.2	60.1

4.5 FIRST STABILITY TESTS

Since it is published in literature¹⁰⁵ that PEA⁺ is not only enhancing solar cell efficiency but also stability of the solar cells, first stability studies of the performance of the triple cation perovskite solar cell devices have been made. The devices were stored under nitrogen atmosphere in a glove box, with H₂O and O₂ values kept under 1 ppm and 4 ppm respectively. Regular IV-measurement, were performed one day after manufacturing and consecutively every 5 – 7 days. Between measurements the device was not illuminated.

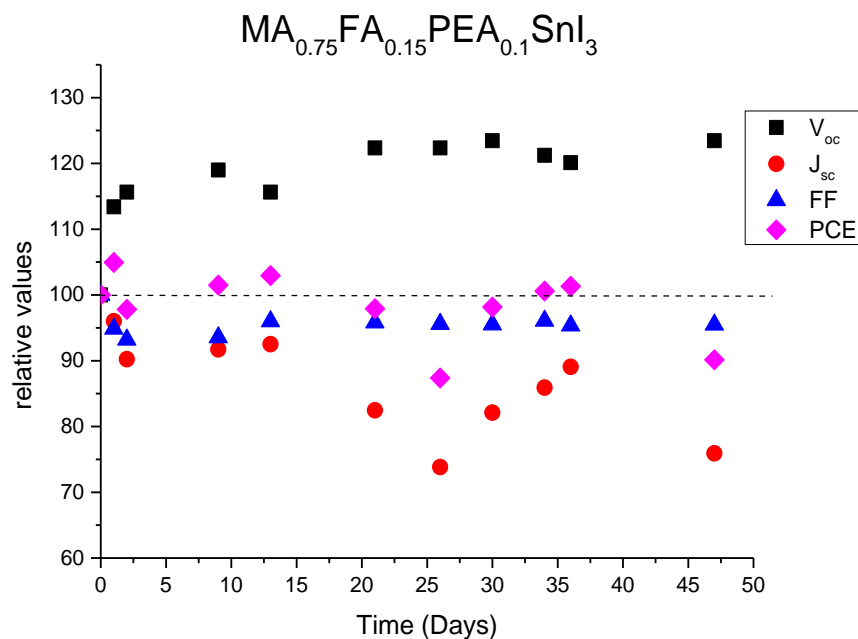


Figure 36: Relative mean values for solar cell performance of triple cation $MA_{0.75}FA_{0.15}PEA_{0.1}SnI_3$ over 7 weeks. Mean values obtained from the best five cells

Device performance values were put into respect to the values obtained at first measurement on day of fabrication, setting this day to day 0. (Fig. 36) V_{oc} started to increase after the first day and stayed, for all the measuring time of 49 days, rather stable at ~120% of initial value. As a consequence of that, PCE also increases and was ~100% for over one month. Values for J_{sc} undergo a heavy drifting from stable 90% to a first minimum of 73% after 26 days, and a regeneration up to 87% after 36 days. Possible reasons could be a change in O₂ concentration during storage or evaporation of solvents. Moreover, a beneficial effect could be the applied electrical field during measurement, which might force the crystalline perovskite phases in a favourable orientation for charge carrier extraction.

Further researched was the direct comparison of double cation $\text{MA}_{0.75}\text{FA}_{0.25}\text{SnI}_3$ to triple cation $\text{MA}_{0.75}\text{FA}_{0.15}\text{PEA}_{0.1}\text{SnI}_3$ in terms of stability, to show the direct beneficial effect of PEA^+ . (Fig. 37)

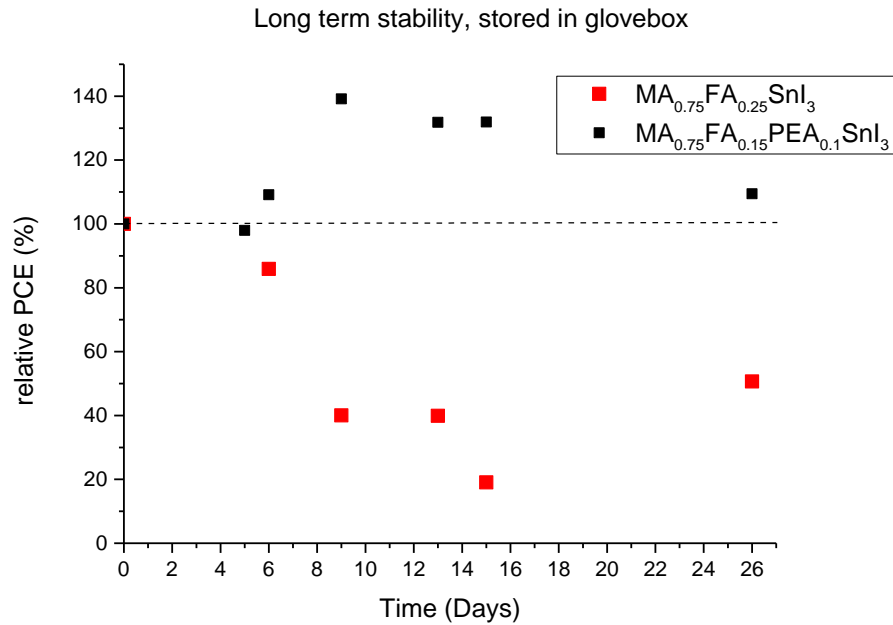


Figure 37: Long term stability of triple cation $\text{MA}_{0.75}\text{FA}_{0.15}\text{PEA}_{0.1}\text{SnI}_3$ compared to double cation $\text{MA}_{0.75}\text{FA}_{0.25}\text{SnI}_3$

For this the PCE values of cells manufactured on the same day and stored under the same circumstances, were compared to each other. The data proves the enhancing effect of PEA^+ on mixed cation tin perovskites. The cells containing PEA^+ not only show a longer lifetime, they are even improved in terms of stability over time. The top cell efficiency was measured 9 days after manufacturing with astonishing 139% of starting PCE. (Tab. 20) Whereas triple cation perovskite improved in its performance, the double cation $\text{MA}_{0.75}\text{FA}_{0.25}\text{SnI}_3$ quickly lost a lot of initial efficiency and dropped to 40% after 9 days. Although regaining some of its performance and reaching 50% of initial PCE after 26 days, $\text{MA}_{0.75}\text{FA}_{0.25}\text{SnI}_3$ still operates at lower efficiency as $\text{MA}_{0.75}\text{FA}_{0.15}\text{PEA}_{0.1}\text{SnI}_3$, which still had 110% of its starting PCE at that time.

Table 20: Highest reached values for triple cation perovskite after 9 days of storage. Mean values over five best cells and best overall cell regarding efficiency

$\text{MA}_{0.75}\text{FA}_{0.15}\text{PEA}_{0.1}\text{SnI}_3$	PCE [%]	Voc [mV]	Jsc [mA/cm^2]	FF [%]
Mean	5.32 ± 0.35	454.6 ± 0.1	20.5 ± 0.6	58.2 ± 2.4
Best	5.63	454.6	21.3	59.3

4.6 INVESTIGATION OF ORGANIC CATION COMBINATIONS

Different organic ammonium iodide salts have been investigated in more detail. Based on the work of Liao et al.¹⁰⁵, where PEA⁺ was added to enhance stability and efficiency (Chapter 2.4.2), other mono- and divalent ammonium salts were added to a FASnI₃ precursor. In this work, n-hexylammonium iodide (HAI), 1,4-benzenediammonium iodide (BDI) and piperazine-1,4-dium iodide (PDI) (Fig. 38) were investigated.

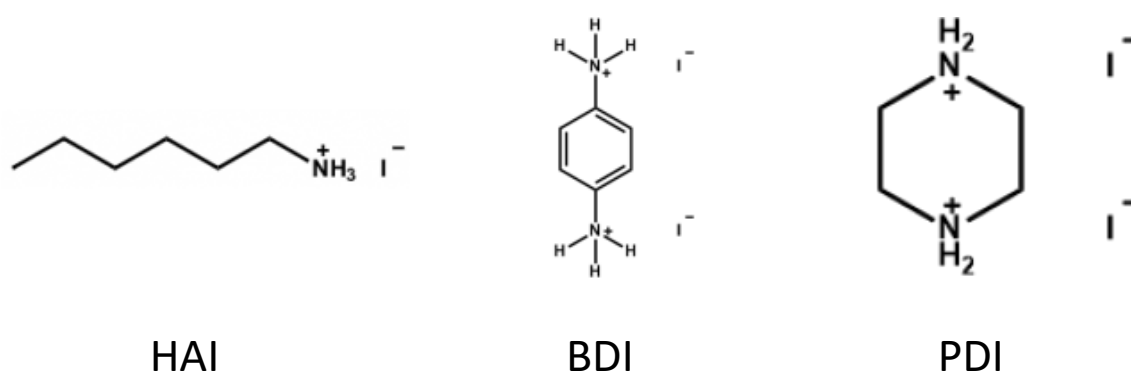


Figure 38: Chemical formula of n-hexylammonium iodide (HAI), 1,4-benzenediammonium iodide (BDI) and piperazine-1,4-dium iodide (PDI)

The idea was that, similar to PEAI, HAI should contribute to the formation of a 2D perovskite structure with an organic separation layer between phases of crystalline FASnI₃. The result however was, that the coating process of PC₆₀BM was hindered, due to no adhesion at the perovskite layer and therefore no ETL could be deposited on the substrate with the given method. This could have been solved with a different ETL, which would be soluble in a more polar solvent, but the solvent should be chosen in a polarity, so that it does not dissolve the perovskite layer again. Since this would have been a more time consuming task, the further development of such a process was not carried out but could be subject to further research. The assumption was made that BDI and PDI might have a similar effect in forming a 2D perovskite structure with an organic linking unit, namely a benzyl in the case of BDI and two ethyl bridges in the case of PDI, between crystalline phases of perovskite. Another possibility would be a 3D loose cross-linked system, where linkage between crystalline perovskite phases forms in all directions. However, it was not possible to produce functioning solar cell devices with the addition of BDI or PDI, due to all fabricated cells rendering a short circuit. More detailed research of the structure and the change in properties of these materials, as well as

testing different device setups, would give more insight into the challenges regarding these materials. Since the further investigation of PEAI was more promising and time was limited a closer investigation of the influence of these cations on the structure and the optical properties was not done.

4.7 INFLUENCE OF SnI_2 PURITY ON SOLAR CELL PERFORMANCE

Since most of the obtained solar cell performance data was much lower than published in literature, a test of the influence of SnI_2 , obtained from different sources was done. This shows how the quality of used SnI_2 has an impact on solar cell performance. SnI_2 from three different sources was tested for its use in triple cation perovskite solar cells. One was used as purchased, one was purified and one was synthesized on our own. The procedure for purification and synthesis is described in chapter 3.2 and 3.3, respectively. As mentioned before the purity of the used SnI_2 plays a significant role in solar cell performance for tin halide perovskite solar power devices, since SnI_4 impurities can be present in commercially available SnI_2 .

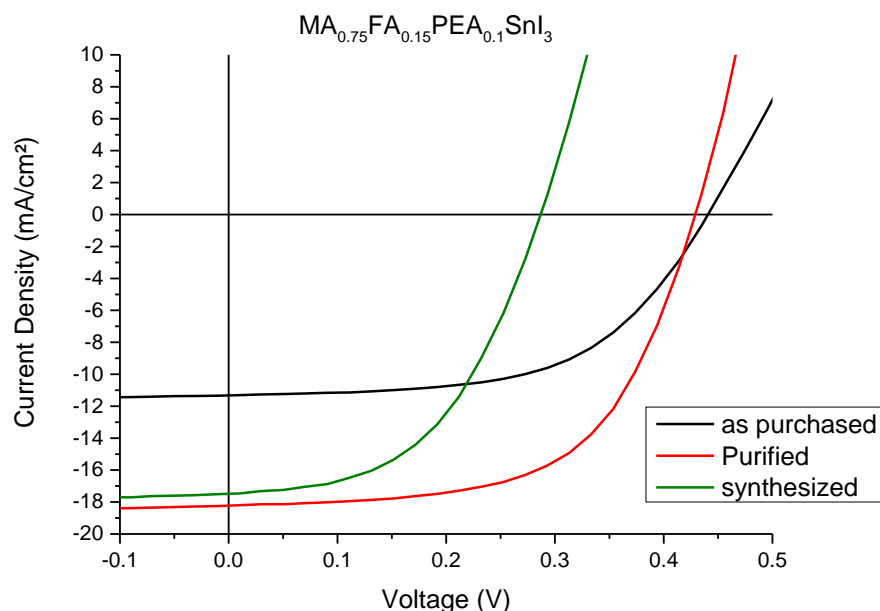


Figure 39: IV-curves of $\text{MA}_{0.75}\text{FA}_{0.15}\text{PEA}_{0.1}\text{SnI}_3$ perovskites with SnI_2 used as purchased, purified and synthesized on our own.

. The measured solar cell characteristics (Fig. 39, Tab. 21) show that the best performance can be obtained with solar cells made from purified SnI_2 . The use of SnI_2 as purchased is not

recommended due to the fact that solar cell devices made from this chemical have the lowest efficiency and lowest values of J_{sc} . One big problem with the purity of the purchased chemical might be long transport routes and multiple possibility to get impurities in contact with the chemicals. However, since distributors guarantee high purity and sealed transport, problems like this should not occur. Further analysis of the received chemicals, which could indicate probable sources of contaminations and the degree of impurity, was not done due to high cost involved in these analysis methods. Although self-made SnI_2 produces cells with high J_{sc} , the values for V_{oc} , are low. Reasons for this might be a significant amount of SnI_4 , which is a by-product of the synthesis route, in the chemical. Since the combination of water and air rapidly oxidises SnI_2 to SnI_4 also errors in handling and reconditioning might strongly influence the purity of the synthesized material. To maintain reproducibility in all devices, purification via sublimation of self-made SnI_2 is recommended for further research.

Table 21: Solar cell performance of $MA_{0.75}FA_{0.15}PEA_{0.1}SnI_3$ perovskites with SnI_2 used as purchased purified and synthesized on our own.

Sample	PCE [%]	Voc [mV]	Jsc [mA/cm ²]	FF [%]
as purchased	2.11 ± 0.41	431.0 ± 7.5	8.5 ± 2.3	59.5 ± 5.5
best	2.83	434.4	11.3	57.7
purified	4.39 ± 0.20	430.3 ± 8.1	17.6 ± 0.7	58.8 ± 2.6
best	4.60	434.3	18.2	59
synthesised	2.29 ± 0.27	280.8 ± 16.2	17.4 ± 1.1	47.0 ± 1.3
best	2.5	293.0	17.5	49.1

5 CONCLUSION AND OUTLOOK

The influence of different cations in tin halide perovskites has been studied in terms of solar cell performance, optical and crystallographic properties, and long term stability. With a solution-based spin coating method, extended with an anti-solvent dropping step, tin halide perovskites have been formed in an inverted device architecture. (ITO/PEDOT:PSS/perovskite/PC₆₀BM/Al) Single cation tin halide perovskites, as CsSnI₃, MASnI₃ and FASnI₃ have been produced and characterized. In terms of optical and crystallographic properties, the experimental data of the fabricated perovskites is in accordance with already published literature.^{90,100,105} This proves that it is possible to obtain the desired perovskites with this fabrication method. Only in the case of CsSnI₃ optical data did not exactly match literature and therefore, it is not sure, if the desired perovskite has formed. However, the chemical behaviour of the purely inorganic CsSnI₃ could be very different to the other inorganic/organic hybrid perovskites investigated in this thesis, and a different fabrication method might achieve better results with this material. Although tin halide perovskites formed with this method, the resulting solar cell performance was far from reported values with the same material.⁹² All in all, a more perovskite type specific method for manufacturing should be investigated for each type of perovskite separately to gain the best possible results. Furthermore, mixed cation perovskites were researched in the above-mentioned categories. The manufacturing route was unchanged and optical and crystallographic data was in accordance in literature in the case of MA_{0.75}FA_{0.25}SnI₃.¹⁰¹ The same problem as in the single cation perovskite occurred also in this case, so even that the desired structure was obtained the solar cell performance was far below already published data.

Moreover, in all perovskite types, the influence of PEA⁺ as enhancing and stabilising cation was closer investigated. Optical absorption shows in all inorganic/organic hybrid materials an increase of absorption or at least no change in absorption properties. This suggests that a small amount of PEA⁺ is enhancing nearly overall absorption in tin halide perovskites and thus is a promising cation to improve the use of these materials in solar cell application. Only in CsSnI₃ the absorption decreases and the onset shifts to lower wavelengths. Except the case of FASnI₃, where band gap values decrease, the band gap energy increases in every investigated sample. This might be an interesting step towards higher V_{oc} values in tin perovskites, since

one major problem in tin-based perovskites is their low open circuit voltage. However, in the change from single cation perovskites to double cation perovskites with PEA^+ , the XRD data was hard to interpret, since almost no literature references were available. It was confirmed, under consideration of the given data, that $\text{FA}_{0.8}\text{PEA}_{0.2}\text{SnI}_3$ and $\text{MA}_{0.8}\text{PEA}_{0.2}\text{SnI}_3$ was formed and the data from the crystallographic diffractogram proves the formation of a 2D structure. The most notable finding originating from these experiments was the fabrication and characterization of the triple cation tin perovskite $\text{MA}_{0.75}\text{FA}_{0.15}\text{PEA}_{0.1}\text{SnI}_3$. Concerning crystallographic properties the obtained data, indicates the formation of 2D structure phases in the material. This newly formed perovskite material exceeded its double cation equivalent in terms of efficiency and long-term stability by far. From this, the enhancing effect of PEA^+ can be seen clearly in all solar cell characteristic. Triple cation solar cells even increased in their efficiency during storage under nitrogen atmosphere and peak at an almost 140% of initial efficiency after 9 days. Further, the solar cells maintained PCE values around 4.6% for over more than a month. Overall, $\text{MA}_{0.75}\text{FA}_{0.15}\text{PEA}_{0.1}\text{SnI}_3$ is a promising new material for solar cell applications and further research regarding this material could result in even better efficiency and stability. If the optimization of the manufacturing process and the composition of cations would be subject of further research, even more advances in the field of tin-based perovskite solar cells could be made.

In addition, another result of this thesis was the influence of the quality of the used chemicals, especially the essential SnI_2 . This study has shown that these chemicals, although purchased with a purity of 99.999%, can be delivered with major impurities. The most common impurity in this material seems to be the oxidised species of the two valent SnI_2 , namely the four valent SnI_4 . Since the oxidation from tin(II)iodide to tin(IV)iodide already occurs during perovskite formation, even in a glovebox with low amounts of water and oxygen, a high concentration of SnI_4 in the starting material is undesirable. Although the chemicals are sealed for transport, purity is not guaranteed, due to the fact that already small amounts of oxygen and water in combination can start the oxidation process. To avoid this kind of problem, most working groups already synthesize their own SnI_2 . Our synthesis pathway has shown that self-made tin(II)iodide is comparable to purchased one, with the benefit of being a lot cheaper. Nonetheless, highest solar cell performance was achieved with SnI_2 purified via resublimation. This method is easy in handling and major impurities, originating from oxidation, can be eliminated during the process.

6 LITERATURE

- 1 REN21, *Renewables 2017 Global Status Report*, Paris, 2017.
- 2 N. Wald and C. Rodeck, *New Dir. Youth Dev.*, 2012, 7–11.
- 3 K. W. Böer, <http://www.chemistryexplained.com/Ru-Sp/Solar-Cells.html>,
State:04.11.2017
- 4 H. Huang and W. Deng, *Introduction to organic Solar cells*, Springer International Publishing, Cham, 2014.
- 5 N. Gupta, G. F. Alapatt, R. Podila, R. Singh and K. F. Poole, *Int. J. Photoenergy*, 2009, **2009**, 1–13.
- 6 R. Couderc, M. Amara and M. Lemiti, *J. Appl. Phys.*, 2014, **115**, 093705.
- 7 J. L. Gray, in *Handbook of Photovoltaic Science and Engineering*, eds. A. Luque and S. Hegedus, John Wiley & Sons, Second edi., 2011.
- 8 S. Güneş and N. S. Sariciftci, in *Printable Solar Cells*, eds. N. D. Sankir and M. Sankir, 2017, pp. 3–36.
- 9 H. Hoppe and N. S. Sariciftci, *J. Mater. Res.*, 2004, **19**, 1924–1945.
- 10 I. D. Parker, *J. Appl. Phys.*, 1994, **75**, 1656–1666.
- 11 V. J. Babu, S. Vempati, S. Sundarrajan, M. Sireesha and S. Ramakrishna, *Sol. Energy*, 2014, **106**, 1–22.
- 12 K. Emery, in *Handbook of Photovoltaic Science and Engineering*, John Wiley & Sons, Ltd, Chichester, UK, 2005, pp. 701–752.
- 13 K. Jager, O. Isabella, A. H. M. Smets, R. A. C. M. M. van Swaaij and M. Zeman, in *SpringerReference*, Springer-Verlag, Berlin/Heidelberg, 2014, pp. 1–420.
- 14 P. Würfel and U. Würfel, *Physics of Solar Cells: From Principles to New Concepts*, WILEY-VCH Verlag, Weinheim, 3rd edn., 2009.
- 15 C. Urich, D. Wynands, S. Olthof, M. K. Riede, K. Leo, S. Sonntag, B. Maennig and M. Pfeiffer, *J. Appl. Phys.*, 2008, **104**, 1–6.

- 16 J. Liu, Y. Shi and Y. Yang, *Adv. Funct. Mater.*, 2001, **11**, 420.
- 17 J. K. J. van Duren, F. Morrissey, C. M. Leewis, K. P. H. Kivits, L. J. van IJzendoorn, M. T. Rispens, J. Hummelen and R. A. J. Janssen, *Adv. Funct. Mater.*, 2002, 679–686.
- 18 C. T. W. Bulle-Lieuwma, J. K. J. van Duren, X. Yang, J. Loos, A. B. Sieval, J. C. Hummelen and R. A. J. Janssen, *Appl. Surf. Sci.*, 2004, **231-2**, 274–277.
- 19 D. M. Chapin, C. S. Fuller and G. L. Pearson, *J. Appl. Phys.*, 1954, **25**, 676–677.
- 20 C. Battaglia, A. Cuevas and S. De Wolf, *Energy Environ. Sci.*, 2016, **9**, 1552–1576.
- 21 I. Tobías, C. del Cañizo and J. Alonso, in *Handbook of Photovoltaic Science and Engineering*, John Wiley & Sons, Ltd, Chichester, UK, 2011, pp. 265–313.
- 22 R. M. Swanson, in *Conference Record of the Thirty-first IEEE Photovoltaic Specialists Conference, 2005.*, IEEE, Lake buena Vista, FL, USA, 2005, pp. 889–894.
- 23 J. I. Pankove and D. A. Kiewit, *J. Electrochem. Soc.*, 1972, **119**, 156C.
- 24 E. Rosencher and B. Vinter, *Cambridge Univ. Press*, 2002, 708.
- 25 M. A. Green, *Prog. Photovoltaics Res. Appl.*, 2002, **10**, 235–241.
- 26 A. Richter, M. Hermle and S. W. Glunz, *IEEE J. Photovoltaics*, 2013, **3**, 1184–1191.
- 27 M. A. Green, Y. Hishikawa, W. Warta, E. D. Dunlop, D. H. Levi, J. Hohl-Ebinger and A. W. H. Ho-Baillie, *Prog. Photovoltaics Res. Appl.*, 2017, **25**, 668–676.
- 28 K. Yoshikawa, H. Kawasaki, W. Yoshida, T. Irie, K. Konishi, K. Nakano, T. Uto, D. Adachi, M. Kanematsu, H. Uzu and K. Yamamoto, 2017, **2**, 17032.
- 29 J. Benick, A. Richter, R. Muller, H. Hauser, F. Feldmann, P. Krenckel, S. Riepe, F. Schindler, M. C. Schubert, M. Hermle, A. W. Bett and S. W. Glunz, *IEEE J. Photovoltaics*, 2017, **7**, 1171–1175.
- 30 T. Matsui, H. Sai, T. Suezaki, M. Matsumoto, K. Saito, I. Yoshida and M. Kondo, in *28th European Photovoltaic Solar Energy Conference and Exhibition*, 2013, pp. 2213 – 2217.
- 31 H. Sai, K. Maejima, T. Matsui, T. Koida, K. Matsubara, M. Kondo, Y. Takeuchi, S. Sugiyama, H. Katayama and I. Yoshida, *IEEE J. Photovoltaics*, 2015, **5**, 1528–1533.

- 32 J. Poortmans and V. Arkhipov, *Thin Film Solar Cells: Fabrication, Characterization and Applications*, John Wiley & Sons, Hoboken, NJ, USA, NJ, USA, 2006.
- 33 R. Birkmire, E. Eser, S. Fields and W. Shafarman, *Prog. Photovoltaics Res. Appl.*, 2005, **13**, 141–148.
- 34 B. E. McCandless and J. R. Sites, in *Handbook of Photovoltaic Science and Engineering*, John Wiley & Sons, Ltd, Chichester, UK, 2011, pp. 600–641.
- 35 H. Binder, *Lexikon der chemischen Elemente*, Hirzel Verlag, Stuttgart, Germany, Germany, 1999.
- 36 A. Tanaka, *Toxicol. Appl. Pharmacol.*, 2004, **198**, 405–411.
- 37 B. M. Kayes, H. Nie, R. Twist, S. G. Spruytte, F. Reinhardt, I. C. Kizilyalli and G. S. Higashi, in *2011 37th IEEE Photovoltaic Specialists Conference*, IEEE, 2011, pp. 000004–000008.
- 38 T. Kato, A. Handa, T. Yagioka, T. Matsuura, K. Yamamoto, S. Higashi, J.-L. Wu, K. F. Tai, H. Hiroi, T. Yoshiyama, T. Sakai and H. Sugimoto, *IEEE J. Photovoltaics*, 2017, **7**, 1773–1780.
- 39 First Solar Press release, *First solar builds the highest efficiency thin film PV cell on record*, 05.08.2014.
- 40 D. J. Friedman, J. M. Olson and S. Kurtz, in *Handbook of Photovoltaic Science and Engineering*, John Wiley & Sons, second edi., 2011, pp. 314 – 364.
- 41 P. T. Chiu, D. L. Law, R. L. Woo, S. Singer, D. Bhusari, W. . Hong, A. Zakaria, J. C. Boisvert, S. Mesropian, R. R. King and N. H. Karam, in *40th IEEE Photovoltaic Specialist Conference*, Denver, 2014, pp. 11–13.
- 42 K. Sasaki, T. Agui, K. Nakaido, N. Takahashi, R. Onitsuka and T. Takamoto, *AIP Conf. Proc.*, 2013, **1556**, 22–25.
- 43 B. M. Kayes, L. Zhang, R. Twist, I.-K. Ding and G. S. Higashi, *IEEE J. Photovoltaics*, 2014, **4**, 729–733.
- 44 M. A. Green, M. J. Keevers, B. Concha-Ramon, Y. Jiang, I. Thomas, J. B. Lasich, P. J. Verlinden, Y. Yang, X. Zhang and K. Emery, in *European Photovoltaic Solar Energy*

- Conference 2015*, Hamburg, 2015, pp. 1 – 5.
- 45 S.-S. Sun and H. O'Neill, in *Handbook of Photovoltaic Science and Engineering*, John Wiley & Sons, Ltd, Chichester, UK, 2011, pp. 675–715.
- 46 D. Beljonne, J. Cornil, V. Coropceanu, D. A. da Silva Filoh, V. Geskin, R. Lazzaroni, P. Leclere and J.-L. Bredas, in *CONJUGATED POLYMERS THEORY, SYNTHESIS, PROPERTIES, AND CHARACTERIZATION*, eds. T. A. Skotheim and J. R. Reynolds., CRC Press, 3rd editio., 2007, pp. 3 – 46.
- 47 M. Knupfer, *Appl. Phys. A Mater. Sci. Process.*, 2003, **77**, 623–626.
- 48 D. M. Balazs, M. J. Speirs and M. A. Loi, in *Organic and hybrid Solar cells*, eds. H. Huang and J. Huang, Springer International Publishing, Cham, 2014, pp. 301–330.
- 49 S. Mori, H. Oh-oka, H. Nakao, T. Gotanda, Y. Nakano, H. Jung, A. Iida, R. Hayase, N. Shida, M. Saito, K. Todorii, T. Asakura, A. Matsui and M. Hosoya, *MRS Proc.*, , DOI:10.1557/opl.2015.540.
- 50 B. O'Regan and M. Gratzel, *Nature*, 1991, **353**, 737–740.
- 51 K. Hara and S. Mori, in *Handbook of Photovoltaic Science and Engineering*, John Wiley & Sons, Ltd, Chichester, UK, 2011, pp. 642–674.
- 52 J. M. Gardner, J. M. Giaimuccio and G. J. Meyer, 2008, **4**, 17252–17253.
- 53 Wikipedia, Dye-sensitized solar cell, https://en.wikipedia.org/wiki/Dye-sensitized_solar_cell. [state: 10.11.2017]
- 54 T. Miyasaka and T. N. Murakami, *Appl. Phys. Lett.*, 2004, **85**, 3932–3934.
- 55 Ecole Polytechnique Fédérale de Lausanne, *ScienceDaily*, 2008.
- 56 R. Komiya, A. Fukui, N. Murofushi, N. Koide, R. Yamanaka, H. Katayama and H., in *21st International Photovoltaic Science and Engineering Conference*, Fukuoka, 2011.
- 57 R. F. Service, *Science.*, 2014, **344**, 458–458.
- 58 M. A. Green, A. Ho-Baillie and H. J. Snaith, *Nat Phot.*, 2014, **8**, 506–514.
- 59 Y. Zhao and K. Zhu, *Chem. Soc. Rev.*, 2016, **45**, 655–689.

- 60 B. Saparov and D. B. Mitzi, *Chem. Rev.*, 2016, **116**, 4558–4596.
- 61 S. D. Stranks, S. D. Stranks, G. E. Eperon, G. Grancini, C. Menelaou, M. J. P. Alcocer, T. Leijtens, L. M. Herz, A. Petrozza and H. J. Snaith, *Science*, 2014, **342**, 341–344.
- 62 J. H. Noh, S. H. Im, J. H. Heo, T. N. Mandal and S. Il Seok, *Nano Lett.*, 2013, **13**, 1764–1769.
- 63 S. F. Hoefler, G. Trimmel and T. Rath, *Monatshefte für Chemie - Chem. Mon.*, 2017, **148**, 795–826.
- 64 K. T. Butler, J. M. Frost and A. Walsh, *Mater. Horiz.*, 2015, **2**, 228–231.
- 65 E. Mosconi, A. Amat, M. K. Nazeeruddin, M. Grätzel and F. De Angelis, *J. Phys. Chem. C*, 2013, **117**, 13902–13913.
- 66 W. J. Yin, Y. Yan and S. H. Wei, *J. Phys. Chem. Lett.*, 2014, **5**, 3625–3631.
- 67 G. Niu, X. Guo and L. Wang, *J. Mater. Chem. A*, 2015, **3**, 8970–8980.
- 68 W. Li, H. Dong, X. Guo, N. Li, J. Li, G. Niu and L. Wang, *J. Mater. Chem. A*, 2014, **2**, 20105–20111.
- 69 I. C. Smith, E. T. Hoke, D. Solis-Ibarra, M. D. McGehee and H. I. Karunadasa, *Angew. Chemie - Int. Ed.*, 2014, **53**, 11232–11235.
- 70 E. T. McClure, M. R. Ball, W. Windl and P. M. Woodward, *Chem. Mater.*, 2016, **28**, 1348–1354.
- 71 A. Babayigit, A. Ethirajan, M. Muller and B. Conings, *Nat. Mater.*, 2016, **15**, 247–251.
- 72 D. Fabini, *J. Phys. Chem. Lett.*, 2015, **6**, 3546–3548.
- 73 D. B. Mitzi, *Inorg. Chem.*, 2000, **39**, 6107–6113.
- 74 F. Hao, C. C. Stoumpos, D. H. Cao, R. P. H. Chang and M. G. Kanatzidis, *Nat. Photonics*, 2014, **8**, 489–494.
- 75 S. Yang, W. Fu, Z. Zhang, H. Chen and C.-Z. Li, *J. Mater. Chem. A*, 2017, **5**, 11462–11482.
- 76 R. D. Shannon, *Acta Crystallogr. Sect. A*, 1976, **32**, 751–767.

- 77 Q. Chen, N. De Marco, Y. Yang, T. Bin Song, C. C. Chen, H. Zhao, Z. Hong, H. Zhou and Y. Yang, *Nano Today*, 2015, **10**, 355–396.
- 78 K. Choudhary, *Appl. Surf. Sci.*, 2015, **334**, 40–44.
- 79 C. C. Stoumpos, L. Frazer, D. J. Clark, Y. S. Kim, S. H. Rhim, A. J. Freeman, J. B. Ketterson, J. I. Jang and M. G. Kanatzidis, *J. Am. Chem. Soc.*, 2015, **137**, 6804–6819.
- 80 T. Krishnamoorthy, H. Ding, C. Yan, W. L. Leong, T. Baikie, Z. Zhang, M. Sherburne, S. Li, M. Asta, N. Mathews and S. G. Mhaisalkar, *J. Mater. Chem. A*, 2015, **3**, 23829–23832.
- 81 W. Ming, H. Shi and M.-H. Du, *J. Mater. Chem. A*, 2016, **4**, 13852–13858.
- 82 L. C. Allen, *J. Am. Chem. Soc.*, 1989, **111**, 9003–9014.
- 83 J.-C. Hebig, I. Kühn, J. Flohre and T. Kirchartz, *ACS Energy Lett.*, 2016, **1**, 309–314.
- 84 P. C. Harikesh, H. K. Mulmudi, B. Ghosh, T. W. Goh, Y. T. Teng, K. Thirumal, M. Lockrey, K. Weber, T. M. Koh, S. Li, S. Mhaisalkar and N. Mathews, *Chem. Mater.*, 2016, **28**, 7496–7504.
- 85 X. Zhang, G. Wu, Z. Gu, B. Guo, W. Liu, S. Yang, T. Ye, C. Chen, W. Tu and H. Chen, *Nano Res.*, 2016, **9**, 2921–2930.
- 86 R. L. Z. Hoyer, R. E. Brandt, A. Osherov, V. Stevanovic, S. D. Stranks, M. W. B. Wilson, H. Kim, A. J. Akey, J. D. Perkins, R. C. Kurchin, J. R. Poindexter, E. N. Wang, M. G. Bawendi, V. Bulovic and T. Buonassisi, *Chem. - A Eur. J.*, 2016, **22**, 2605–2610.
- 87 T. Kawai, A. Ishii, T. Kitamuha, S. Shimanuki, M. Iwata and Y. Ishibashi, *J. Phys. Soc. Japan*, 1996, **65**, 1464–1468.
- 88 S. Öz, J.-C. Hebig, E. Jung, T. Singh, A. Lepcha, S. Olthof, F. Jan, Y. Gao, R. German, P. H. M. van Loosdrecht, K. Meerholz, T. Kirchartz and S. Mathur, *Sol. Energy Mater. Sol. Cells*, 2016, **158**, 195–201.
- 89 B. W. Park, B. Philippe, X. Zhang, H. Rensmo, G. Boschloo and E. M. J. Johansson, *Adv. Mater.*, 2015, **27**, 6806–6813.
- 90 C. C. Stoumpos, C. D. Malliakas and M. G. Kanatzidis, *ACS Inorg. Chem.*, 2013, **52**,

- 9019–9038.
- 91 C. R. Kagan, *Science.*, 1999, **286**, 945–947.
- 92 M. Konstantakou, T. Stergiopoulos, C. Wang, W. Liao, N. Shrestha, C. R. Grice, A. J. Cimaroli, L. Guan, R. J. Ellingson, K. Zhu, X. Zhao, R.-G. Xiong, Y. Yan, D.-H. Kim, H. J. Snaith, R. J. Sutton, W. Ma, F. Moghadam, B. Conings, A. Babayigit, H.-G. Boyen, S. Bent, F. Giustino, L. M. Herz, M. B. Johnston, M. D. McGehee and H. J. Snaith, *J. Mater. Chem. A*, 2017, **2**, 17018.
- 93 F. Hao, C. C. Stoumpos, P. Guo, N. Zhou, T. J. Marks, R. P. H. Chang and M. G. Kanatzidis, *J. Am. Chem. Soc.*, 2015, **137**, 11445–11452.
- 94 I. Chung, B. Lee, J. He, R. P. H. Chang and M. G. Kanatzidis, *Nature*, 2012, **485**, 486–9.
- 95 M. H. Kumar, S. Dharani, W. L. Leong, P. P. Boix, R. R. Prabhakar, T. Baikie, C. Shi, H. Ding, R. Ramesh, M. Asta, M. Graetzel, S. G. Mhaisalkar and N. Mathews, *Adv. Mater.*, 2014, **26**, 7122–7127.
- 96 H. Do Kim, Y. Miyamoto, H. Kubota, T. Yamanari and H. Ohkita, *Chem. Lett.*, 2017, **46**, 253–256.
- 97 L. Ma, F. Hao, C. C. Stoumpos, B. T. Phelan, M. R. Wasielewski and M. G. Kanatzidis, *J. Am. Chem. Soc.*, 2016, **138**, 14750–14755.
- 98 N. K. Noel, S. D. Stranks, A. Abate, C. Wehrenfennig, S. Guarnera, A.-A. Haghighirad, A. Sadhanala, G. E. Eperon, S. K. Pathak, M. B. Johnston, A. Petrozza, L. M. Herz and H. J. Snaith, *Energy Environ. Sci.*, 2014, **7**, 3061–3068.
- 99 W. Ke, C. C. Stoumpos, M. Zhu, L. Mao, I. Spanopoulos, J. Liu, O. Y. Kontsevoi, M. Chen, D. Sarma, Y. Zhang, M. R. Wasielewski and M. G. Kanatzidis, *Sci. Adv.*, 2017, **3**, e1701293.
- 100 W. Liao, D. Zhao, Y. Yu, C. R. Grice, C. Wang, A. J. Cimaroli, P. Schulz, W. Meng, K. Zhu, R. G. Xiong and Y. Yan, *Adv. Mater.*, 2016, **28**, 9333–9340.
- 101 Z. Zhao, F. Gu, Y. Li, W. Sun, S. Ye, H. Rao, Z. Liu, Z. Bian and C. Huang, *Adv. Sci.*, 2017, **4**, 1 – 7.
- 102 B. Zhao, M. Abdi-Jalebi, M. Tabachnyk, H. Glass, V. S. Kamboj, W. Nie, A. J. Pearson, Y.

- Puttisong, K. C. Gödel, H. E. Beere, D. A. Ritchie, A. D. Mohite, S. E. Dutton, R. H. Friend and A. Sadhanala, *Adv. Mater.*, 2017, **29**, 1604744.
- 103 T. K. Todorov, K. B. Reuter and D. B. Mitzi, *Adv. Mater.*, 2010, **22**, E156–E159.
- 104 D. B. Mitzi, S. Wang, C. A. Feild, C. A. Chess and A. M. Guloy, *Science.*, 1995, **267**, 1473 – 1476.
- 105 Y. Liao, H. Liu, W. Zhou, D. Yang, Y. Shang, Z. Shi, B. Li, X. Jiang, L. Zhang, L. N. Quan, R. Quintero-Bermudez, B. R. Sutherland, Q. Mi, E. H. Sargent and Z. Ning, *J. Am. Chem. Soc.*, 2017, **139**, 6693–6699.
- 106 S. Shao, J. Liu, G. Portale, H. Fang, G. R. Blake, G. H. ten Brink, L. J. A. Koster and M. A. Loi, *Adv. Energy Mater.*, 2017, **7**, 1702019.
- 107 S. J. Lee, S. S. Shin, Y. C. Kim, D. Kim, T. K. Ahn, J. H. Noh, J. Seo and S. Il Seok, *J. Am. Chem. Soc.*, 2016, **138**, 3974–7.
- 108 K. P. Marshall, M. Walker, R. I. Walton and R. A. Hatton, *Nat. Energy*, 2016, **1**, 16178.
- 109 T. M. Koh, T. Krishnamoorthy, N. Yantara, C. Shi, W. L. Leong, P. P. Boix, A. C. Grimsdale, S. G. Mhaisalkar and N. Mathews, *J. Mater. Chem. A*, 2015, **3**, 14996–15000.

7 INDEX OF FIGURES

Figure 1: Renewable energy share of Global electricity production. End 2016	1
Figure 2: Basic scheme of a p–n–junction solar cell and charge transport phenomena ⁵	4
Figure 3: p–n–junction with Fermi–levels changed by doping (a) and alignment when in contact (b)	5
Figure 4: Schematic visualisation of charge carrier transport in organic semiconductors, with electrons (e ⁻) and holes (h ⁺) diffusion towards the respective current collectors	5
Figure 5: Schematic illustration of a typical IV – measurement	7
Figure 6: scheme of a modern crystalline silicon cell	10
Figure 7: schematic setup of solar cell devices for a) CIGS cells and b) CdTe cells.....	11
Figure 8: triple – junction solar cell, composed of Ge bottom cell, GaAs as middle cell and GaInP as top cell, with correlating absorbance in the solar spectrum.....	12
Figure 9: schematic device setup of an organic solar cell in bilayer and bulk heterojunction system.	14
Figure 10: chemical structure of P3HT and PCBM	15
Figure 11: schematic function principle of a dye sensitised solar cell. Original work by M. R. Jones ⁵³	16
Figure 12: schematic perovskite structure, with A= monovalent cation, B= divalent cation and X= monovalent halide anion ⁵⁸	17
Figure 13: schematic device setup of a perovskite solar cell. HTM= hole transport material ETM= electron transport material	18
Figure 14: Schematic illustration of 2D structured PEA _{0.2} FA _{0.8} SnI ₃ perovskite on NiO substrate ¹⁰⁵ and chemical structure of PEAI.....	25
Figure 15: Schematic architecture of one solar cell.....	28
Figure 16: UV/Vis absorption spectra of single cation Sn – perovskites.....	31
Figure 17: Tauc–plot of single cation Sn–perovskites.....	33
Figure 18. XRD diffractogram of MASnI ₃	34
Figure 19: XRD diffractogram of FASnI ₃	34
Figure 20: IV–curves of single cation Sn–perovskites	35
Figure 21: UV/Vis absorption of MA _{0.75} FA _{0.25} SnI ₃ perovskite	37
Figure 22: Tauc–plot of MA _{0.75} FA _{0.25} SnI ₃ perovskite	38
Figure 23: XRD-diffractograms of MA _{0.75} FA _{0.25} SnI ₃ perovskite	39

Figure 24: IV – curves of MA _{0.75} FA _{0.25} SnI ₃ perovskite, measurements in the dark and under illumination	40
Figure 25: Absorption spectra of a) CsSnI ₃ b) MASnI ₃ and c) FASnI ₃ and their corresponding absorption with 20 mol% PEA ⁺ substitution	41
Figure 26: Band gap values of a) CsSnI ₃ b) MASnI ₃ and c) FASnI ₃ and their corresponding mixed cation equivalent with 20 mol% PEA ⁺ substitution.....	42
Figure 27: XRD diffractograms of FA _{0.8} PEA _{0.2} SnI ₃ perovskite compared to FASnI ₃	43
Figure 28: XRD diffractograms of MA _{0.8} PEA _{0.2} SnI ₃ perovskite compared to MASnI ₃	44
Figure 29: IV–curves of A _{0.8} PEA _{0.2} SnI ₃ (A= Cs, MA, FA) mixed cation perovskites.....	45
Figure 30: UV/Vis absorption of triple cation MA _{0.75} FA _{0.15} PEA _{0.1} SnI ₃ compared to double cation MA _{0.75} FA _{0.25} SnI ₃	47
Figure 31: Band gap energies of triple cation MA _{0.75} FA _{0.15} PEA _{0.1} SnI ₃ compared to double cation MA _{0.75} FA _{0.25} SnI ₃	48
Figure 32: XRD diffractograms of triple cation MA _{0.75} FA _{0.15} PEA _{0.1} SnI ₃ compared to double cation MA _{0.75} FA _{0.25} SnI ₃	49
Figure 33: IV curves of MA _{0.75} FA _{0.15} PEA _{0.1} SnI ₃ and MA _{0.75} FA _{0.05} PEA _{0.2} SnI ₃	50
Figure 34: EQE measurement results of MA _{0.75} FA _{0.15} PEA _{0.1} SnI ₃	51
Figure 35: Hysteresis behaviour of triple cation MA _{0.75} FA _{0.15} PEA _{0.1} SnI ₃	52
Figure 36: Relative mean values for solar cell performance of triple cation MA _{0.75} FA _{0.15} PEA _{0.1} SnI ₃ over 7 weeks. Mean values obtained from the best five cells.....	53
Figure 37: Long term stability of triple cation MA _{0.75} FA _{0.15} PEA _{0.1} SnI ₃ compared to double cation MA _{0.75} FA _{0.25} SnI ₃	54
Figure 38: Chemical formula of n–hexylammonium iodide (HAI), 1,4-benzenediammonium iodide (BDI) and piperazine-1,4-dium iodide (PDI)	55
Figure 39: IV –curves of MA _{0.75} FA _{0.15} PEA _{0.1} SnI ₃ perovskites with SnI ₂ used as purchased, purified and synthesized on our own.....	56

8 INDEX OF TABLES

Table 1: solar cell characteristics of different types of silicon solar cells. Publisher abbreviations: FhG – ISE: Fraunhofer Institut für Solare Energiesysteme, AIST: Japanese National Institute of Advanced Industrial Science and Technology ²⁷	10
Table 2: solar cell performance of state of the arts thin film solar cells. [state 2017] ²⁷	12
Table 3: III – V semiconductor multi – junction device performances ²⁷	13
Table 4: best efficiency of organic solar cell [state:2017] ²⁷	15
Table 5: best performance of a DSSC [state: 2017] ²⁷	16
Table 6: Ge – perovskite solar cell performance ⁸¹	20
Table 7: most promising solar cell performance for Sb – based PSCs ⁶⁴	21
Table 8: performance of MA ₃ Bi ₂ I ₉ and Cs ₃ Bi ₂ I ₉ PSCs in different device setups ⁶⁴	22
Table 9: PV performance of best Sn – perovskite solar cells build with DSSC device setup ⁹³ .	24
Table 10: PV performance of best Sn – perovskite solar cells build with inverted device setup ⁹³	24
Table 11: Layer thickness values of single cation tin perovskites, mean values and standard deviation.....	32
Table 12: Band gap values for tin perovskites, experimental data and literature values ^{96,99,110}	33
Table 13: Mean solar cell parameters of single cation tin perovskites. Mean values were obtained from five best cells. Best cell values were chosen in with regards to highest efficiency.	36
Table 14: Best Sn – based perovskite solar cell performance published in literature.....	37
Table 15: Solar cell characteristics of MA _{0.75} FA _{0.25} SnI ₃ perovskite. Mean values were obtained from five best cells. Best cell values were chosen in with regards to highest efficiency	40
Table 16: perovskite layer thickness of A _{0.8} PEA _{0.2} SnI ₃ (A= Cs, MA, FA)	42
Table 17: solar cell characteristics of A _{0.8} PEA _{0.2} SnI ₃ (A= Cs, MA, FA) mixed cation perovskites and best cell values. Mean values were obtained from five best cells. Best cell values were chosen in with regards to highest efficiency.....	46
Table 18: solar cell characteristics of triple cation perovskites. Mean values were obtained from five best cells. Best cell values were chosen in with regards to highest efficiency	50
Table 19: solar cell performance triple cation MA _{0.75} FA _{0.15} PEA _{0.1} SnI ₃ in forward and backward bias. Mean values of best five cells. Best cell values was taken regarding best efficiency	52

Table 20: Highest reached values for triple cation perovskite after 9 days of storage. Mean values over five best cells and best overall cell regarding efficiency 54

Table 21: Solar cell performance of $\text{MA}_{0.75}\text{FA}_{0.15}\text{PEA}_{0.1}\text{SnI}_3$ perovskites with SnI_2 used as purchased purified and synthesized on our own..... 57